FORSCHUNGSZENTRUM JÜLICH GmbH

Institut für Plasmaphysik
Association EURATOM-KFA

Interaction of Pellets with Hot Plasmas

K.H. Finken

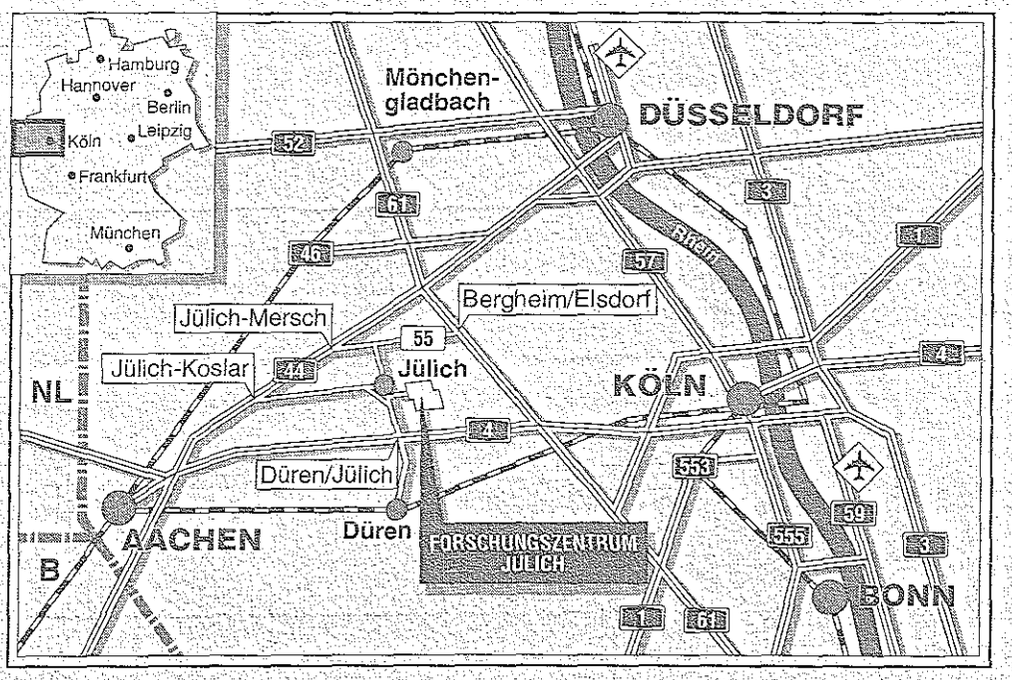

Berichte des Forschungszentrums Jülich ; 2980
ISSN 0944-2952
Institut für Plasmaphysik Jül-2980
Association EURATOM-KFA

Zu beziehen durch: Forschungszentrum Jülich GmbH · Zentralbibliothek
D-52425 Jülich · Bundesrepublik Deutschland
Telefon: 02461/61-6102 · Telefax: 02461/61-6103 · Telex: 833556-70 kfa d

Interaction of Pellets with Hot Plasmas

K.H. Finken

Contents

I. Introduction

In thermonuclear fusion research, pellet plasma interaction occurs in two important areas: One is the so-called inertial confinement and the second one is the injection of pellets in a magnetically confined plasma. In inertial confinement, a spherical target of a few millimeters diameter filled with a deuterium-tritium mixture - the pellet - is bombarded with a well focussed high power beam of either photons (laser-beam, indirectly by laser beam initiated incoherent X-ray radiation) or particles (electron-, light ion- or heavy ion-beam). The beam energy has to be in the order of Mega-Joule for a time span of several nanoseconds. The beam heats the outer surface of the pellet and forms an expanding plasma cloud. The expansion establishes a reaction-force directed towards the pellet center and initiates a compression wave into the pellet. To reach a positive energy balance, i.e. to extract more fusion power from the pellet than has been put in by the beam, it is necessary to compress the pellet center to a density of over one thousand times the solid state density. Under this condition the inertia of the pellet matter keeps the material together long enough for obtaining the desired burning rate. Inertial confinement attracts much attention from the military side and, therefore, some aspects are still classified. In the following, inertial confinement will not be discussed.

The primary goal of the pellet injection into magnetically confined plasmas is the fuelling of the discharge. Here, the pellets are hydrogen or deuterium ice pieces with a volume of typically a few cubic-millimeters; the number of atoms of such pellets is a substantial fraction of the total number of particles in the discharge. Fuelling by pellet injection is complementary to the conventionally used

gas injection fuelling. The fuelling allows the stationary regulation of a discharge density, if the device has a balanced particle sink. In short pulse machines the sink is either simply the wall, a pumped limiter or a pumped divertor. In long pulse discharges like the planned ITER device, wall pumping eventually saturates, so that active exhaust systems are necessary. Gas injection has the disadvantage, that the ionization processes take place close to the plasma edge. This leads to a strong reduction of the probability for the fuelling gas to penetrate into the central plasma. The gas remains at the plasma boundary; this is equivalent to a low fuelling efficiency and a high neutral particle pressure at the plasma boundary. The low fuelling efficiency in a fusion reactor means that an undesired high amount of tritium gas has to be introduced into the machine; the tritium recycles in the plasma boundary of the discharge and is extracted together with the helium ash. The high recycling is connected with a high gas pressure at the plasma edge and this high neutral density deteriorates the plasma confinement. This negative effect can be avoided by injecting a pellet deeply into a fusion plasma. The influence of the pellet injection on the plasma performance will be discussed in chapter III. In chapter II the effects directly associated with the penetration into the discharge are treated.

The injection of pellets into a plasma leads to an enormous heat transfer from the plasma to the pellet. For "normal" heat fluxes, the heat deposition to a solid surface and the heat propagation into the solid is described by the well-known heat equation. If, however, the incoming heat flux is so high that the surface material is evaporated before the heat sufficiently penetrates into the bulk, a new effect, the so-called 'gas shielding', is observed. In everyday life this effect is

known as the Leidenfrost phenomenon /I.1, I.2/ and it occurs if e.g. a droplet of water falls on a hot plate. The water contracts to a ball so that the contact surface to the hot plate is minimum. The calefaction leads to the formation of a vapor cloud at the contact point, which lifts the droplet from the hot plate and inhibits the heat transition by orders of magnitude.

If the shielding effect would be neglected and it would be assumed that the water (1 mm thick) remains in contact to e.g. a 500 ^{o} C plate, then the droplet would evaporate within less than a second. The actual evaporation time of the droplet is extended because during extreme heating the evaporation from the surface leads to an isolating protection gas film between the plate and the droplet. Some properties of the Leidenfrost phenomenon are very specific and cannot be generalized like e.g. the flow pattern of the gas layer supporting the droplet from the hot plate. Other features like the protection cloud, however, are so general that they are also of importance for the pellet ablation process in the plasma.

II. Pellet Ablation

II.A Interaction of Single Particles with Solid Hydrogen

Before coming to the ablation models, first the interaction processes between incoming single particles of different energies with a hydrogen (ice) target are discussed. For most conditions in a magnetic fusion device, the largest fraction of the energy is transported and deposited by the electrons from the hot plasma to the pellet; the ions are shielded effictively by the cloud and the photon density in typical fusion plasmas is too low. An important exception may be discharges with high neutral beam heating power /see III.D/. The interaction between a beam

and hydrogen is characterized by the stopping cross section (-dE/dx). Fig. II.1 gives an overviev of the stopping cross section for electron impact and proton impact on a H_2 (provided by J. Schou). At particle energies below 0.5 keV the electron cross section dominant and at higher energies the influence of the ions becomes dominant. The stopping power taken from Anderson and Ziegler agrees well with the curves from Børgeson ans Søreson except for the Deuterium-Deuterium case. The reason for the discrepancy is not yet known.

An electron beam injected into a solid target is attenuated both by inelastic collisions with the electrons in the solid, which leads to excitation and ionization processes, and by elastic collisions with the atomic nuclei. The beam particle interaction is treated in review articles /II.A.1, II.A.2/. For the hydrogen target each ion-electron ionization pair requires an energy of about 38 eV /II.A.3/.

The penetration depth into solid hydrogen or the mean projected range R of an electron beam in the keV range has been investigated by Valkealahti et al. /II.A.4/ and it can be described as

$$\frac{R}{[10^{15}\text{molecules/cm}^2]} = 0.53 \cdot \left(\frac{E}{[\text{keV}]}\right)^{1.72} \qquad \text{(II.1)}$$

This value is derived from computer code calculations and includes scattering on nuclei; it is 1/0.75 times larger than the value in the gas phase. According to this formula electrons of 1 keV have a range of $n \cdot l \approx 5.3 \cdot 10^{17}$ molecules/cm^2 which is equivalent to $\rho \cdot l \approx 1.7 \cdot 10^{-5}$ g/cm^2 or a penetration depth of about $2 \cdot 10^{-4}$ cm in condensed hydrogen. It will be shown later that by far most of these electrons (99.99 % /1.E.14/) are absorbed from the ablated cloud and do not reach the pellet

surface. High energy electrons in the 100 keV range are produced in low and medium density tokamak discharges, where e.g. resonant waves, launched from the outside, accelerate a group of electrons, so that these particles carry most of the plasma current ("slide away" electrons) - so-called current drive experiments. Under these conditions, the electrons penetrate through the cloud and deposit their energy inside the pellets. This can lead to a quick destruction of the pellets. Finally, runaway electrons with an energy of several MeV can be created in discharges with very low electron densities ($n_e \leq 10^{19}$ m^{-3}); these electrons can pass the pellet without destroying it.

If the effect of the cloud can be neglected, the erosion due to sputtering can be studied /II.A.5/. Measurements performed at an electron energy of 2 keV show that one incoming electron sputters about 10 hydrogen atoms from a target. The collision rate of the plasma ions with the pellet target is by the factor $(m_e / m_i)^{1/2}$ smaller than the electron collision rate. Nevertheless, the sputtering due to ions is more effective because the sputtering yield of ions amounts to 10^3 atoms per incoming ion /II.A.6, II.A.7/. The sputtering is primarily not based on knock on collisions with the nuicei like in most other materials but due to electrnic excitation and subsequent decay into repulsive states; it is effective because the binding energy, which is equal to the sublimation energy, is very low and ranges from 8.655 meV for solid H_2 to 14.8 meV for T_2.

If a typical pellet with a hydrogen content of about $5 \cdot 10^{20}$ atoms is injected into a hot plasma, its observed lifetime there amounts to about 0.5 ms. This corresponds to an erosion rate of about 10^{24} s^{-1}. We compare this erosion rate to the value estimated from the sputtering yields of electrons and ions. A plasma in

a typical tokamak has a density of $n_e \approx 5 \cdot 10^{19}$ m^{-3} and an electron temperature $T_e \approx 1$ keV. This plasma surrounds a 1 mm pellet; this leads to a collision rate of $\nu^{coll} = n \cdot \nu_{ther} \cdot A_{pellet} \approx 10^{21}$ s^{-1} for electrons and $2.5 \cdot 10^{19}$ s^{-1} for the ions. The erosion rates due to pure sputtering without the shielding effect of the cloud would then amount to about 10^{22} s^{-1} for electrons and $2.5 \cdot 10^{22}$ s^{-1} for ions. These values are 1 to 2 orders of magnitude lower than observed during the ablation. As the cloud shielding is neglected, this is an upper limit estimate for the erosion due to sputtering and it shows that sputtering should not be the dominant erosion process. The dominant process is assumed to be evaporation.

There is an interesting aspect of charged particle interaction that is normally not considered during the ablation process in the plasma: The solid deuterium emits light in response to the particle interaction /II.A.9, II.A.10/. The light is emitted as a broad continuum band in the red and near infra red spectral region, but not coincident with the H_a line.

II.B Ablation Models

If a solid hydrogen ice pellet is suddenly exposed to the plasma, it will be heated mainly by particle impact. The particles from the plasma deposit their energy close to the surface such that a rapid evaporation and/or sputtering is initiated. The ablated particles are predominantly neutral in the beginning. They start to expand without restrictions due to electrical or magnetic fields and form a spherical cloud. The cloud expands freely until ionization processes become dominant. The cloud diameter is then on the order of one centimeter. The ionized shell surrounding the cloud is subjected to the influence of the local magnetic and

electric fields in the tokamak. An overview about the power fluxes crossing the outer ionized shell surface, the surface of the neutral cloud (thermal electrons and fast electrons separately) and the pellet surface are plotted in fig. II.2 for a pellet penetrating from the outside of the discharge to the axis /II.E.14/. The peak value entering the outermost surface amounts to about 40 MW (450 J during pellet-lifetime); 10% of this flux reaches the neutral cloud and only 0.01 of the flux reaching the neutral cloud arrives at the pellet surface. So the incoming flux is in total reduced by about three orders of magnitude.

An early description of this ablation process is the so-called "Neutral Gas Shielding", NGS - model of Parks and Turnbull /II.B.1, II.B.2/ which has been extended by Milora and Foster /II.B.3, II.B.4/, Chang et al./II.B.5, II.B.7/, Houlberg et al. /II.B.8/ and Lengyel/II.B.9 - II.B.13/ and others /II.B.14 - II.B.17/. The development time of a shielding cloud amounts to about 0.1 μs, the expansion time along the magnetic field about 1-2 μs and the crossing of a pellet with v = 1 km/s through the cloud to about 25 μs; all these times are fast compared to the pellet ablation time of typically 0.5 ms. Therefore, the ablation process is seen as quasi steady state. The hydrodynamic conservation equations of mass, momentum and energy are solved for a 1D spherically expanding gas flow. The pellet surface is the source, its temperature is assumed to be $T \approx 0$ K. The plasma electrons hitting the cloud deposit their energy in the cloud. This energy is mainly used to heat up, ionize and accelerate the ablated gas radially outwards. Only a very small fraction of the incoming energy provides the energy for the evaporation of the pellet surface.

Newer models have extended this 'Neutral Gas Shielding' model without

drastically changing the old result. The most important changes are: The incoming electrons are no longer mono-energetic but a more realistic distribution is allowed /II.B.18/; plasma effects like the deformation of the magnetic field and plasma shielding /II.B.8, II.B.12, II.B.19/ are added to the model by different authors. An example of the radial distribution of the neutral mass density, the electron density and ion and electron temperature is shown in fig. II.3. The application of pellets for reactor fuelling is studied in /II.B.7, II.B.20 and IV.2/.

II.C Ablation Rate

The aim of the pellet ablation models is to predict the local ablation rate of a pellet, its penetration depth and sometimes details like the flow pattern of the ablated gas, its ionization rate and the H_α emission from the ablated gas. The different models predict slightly different results. A recent study by Houlberg on JET /II.C.1/ gave the following predictions on the ablation rate and the penetration depth: When a pellet (radius r_p, molecular density of solid hydrogen $n_m \approx 2.1 \cdot 10^{28}$ m^{-3}, atomic mass number of the pellet material (H, D or T) A_p) is injected into a background plasma of density n_e and electron temperature T_e, the pellet radius diminishes as:

$$-\frac{dr_p}{dt} \propto \frac{n_e^{1/3} \cdot T_e^{5/3}}{A_p^{1/3} \cdot n_m \cdot r_p^{2/3}} \qquad \text{(II.2)}$$

The equation shows that the decrease of the pellet radius, which stands here also for the ablation rate, depends very strongly on the electron temperature of the plasma and only to a minor degree on the plasma density. Therefore, a pellet

penetrates deeper into a high density - lower temperature - plasma than into a low density plasma, which has generally the higher temperature. The integration of dr_p/dt over the pellet path, until r_p becomes zero, gives the penetration depth λ of the pellet into the plasma.

II.D Penetration Depth of the Pellet

For this integration the initial plasma density and temperature distribution must be known. For estimations of the penetration depth λ, the following plasma profiles are assumed:

$$n_e(x) = n_{eo} \cdot (1-x)^{e_n} ; \quad T_e(x) = T_{eo} \cdot (1-x)^{e_T} \qquad \text{(II.3)}$$

where n_{eo} and T_{eo} correspond to the central electron densities and temperatures, and a is the minor radius of the plasma and $x = r/a$ is the normalized radius. The exponents are free parameters which have to be fitted to the experimentally determined distributions. The time in the integral is transformed to one over the pellet path with

$$dt = -\frac{a}{v_p} \cdot dx \qquad \text{(II.4)}$$

where v_p is the pellet velocity. With these assumptions the penetration depth λ becomes /II.C.1/:

$$\frac{\lambda}{a} \propto \left(\frac{v_p \, n_m \, A_p^{1/3} \, r_{po}^{5/3}}{a \, n_{eo}^{1/3} \, T_{eo}^{5/3}} \right)^{\beta_{ngs}} \qquad \text{(II.5)}$$

here r_{po} is the initial pellet radius and $\beta_{ngs} = 3/(3 + \alpha_n + 5\alpha_T)$. For linear profiles the α-values are $\alpha_n = \alpha_T = 1$, and consequently $\beta_{ngs} = 1/3$. The equation shows that the strongest influence on the penetration depth is due to the initial pellet size r_{po} and the electron temperature T_e. The influence of the pellet velocity on the penetration depth is weaker.

The ablation models predict further that the electron density in the ablation zone reaches values up to 10^{22} to 10^{23} m^{-3} /II.D.1/. This value is determined by the balance of the ablation rate and of the streaming velocity of the ablated gas. The dependence of the neutral gas density, the electron density, the electron temperature and the ion temperature as a function of the distance from the pellet center are shown in fig. II.3. The transport of the ablated pellet material is predicted to occur predominantly parallel to the magnetic field lines; the streaming velocity far away from the pellet is in the order of the sound speed or slightly higher.

II.E Experimental Observations of the Ablating Pellet.

The pellet penetration depth into the plasma is one of the observations which allow a comparison with the model predictions. Recent experiments performed at JET /II.C.1 II.E.1 II.E.2/ show a remarkably good agreement between the observed penetration depth λ and the simple neutral gas shielding (NGS) model. In these experiments, the size dependence and velocity dependence have been investigated /II.E.3, II.E.4/. The observed pellet penetration scaling, however,

shows slight differences between different machines. The reason for this difference is not yet identified, but it is under discussion whether it can be attributed either to the different pellet size or to the magnetic field in the different devices. Examples from other experiments are listed in ref. /II.E.5 -II.E.10, II.E.14/

A more detailed comparison of the ablation models is performed by the analysis of the pellet ablation rate during its passage into the plasma. The ablation rate can be measured by two means: a) by the difference in the electron density profile immediately before and after the pellet injection and b) by the D_α and D_β light emission occurring from ionization / excitation processes during the pellet ablation.

Experiments on JET and TFTR /II.E.1 II.E.2/ have shown that the ablation rates determined by the two techniques disagree strongly. The results from JET are shown in fig. II.4. The picture shows the density distribution before and after the pellet injection and the difference between these data (top part). In the lower part of the figure, the ablation rate according to methods a) and b) and a value from the gas shielding model are shown. The D_α method shows the ablation maximum of the pellet occurs in the central plasma, which here is also the end of the pellet path. The ablation maximum deduced from method a) is considerably nearer to the plasma edge. The prediction of the NGS-model would favor the result from measurement b), but the authors stated that the D_α-emission intensity is not proportional to the ablation rate as is assumed by many other authors /II.B.6, II.E.11/. The statement is based on D_α emission calculations by /II.D.1/ where the collisional excitation and radiative de-excitation are balanced. For the plasma conditions in the ablating cloud the D_α emission seems, according to /II.E.2/, to be

more closely related to the heat flux incident on the pellet than to the effective ablation rate, as is shown in fig. II.5. Even though the pellet ablation rate as a function of the pellet position agrees only poorly with the observation, the total penetration depth agrees well with the predicted value from the NGS-theory.

For the pellet cloud, a stationary state with a spherically symmetric gas flow is assumed. The gas is ionized at the outer boundary and mixes with the background plasma. Some local parameters such as the electron density and electron temperature can be measured by spectroscopic means such as line broadening and line ratios. Several experiments have been performed on TFR and TFTR. Fig. II.6 shows results from TFR /II.E.12/ about electron density, temperature and the number of ablated deuterium ions in the atomic state $n=4$ along the cloud (striation see also II.F and III.J). It was found that the electron density is in the order of 10^{23} m^{-3} and the electron temperature near the ionization zone is on the order of 1.5 - 2 eV. These values agree well with the expectations.

Measurements on the toroidal expansion of the ablated pellet plasma have been performed on TFTR and JET by determining the density propagation on different positions around the torus. The density pulse propagates toroidally with a velocity of the order of $1.5 \cdot 10^3$ m/s which is of the expected order of the Mach number $M \geq 1$ /II.E.2/. In T-10 also a poloidal propagation with a velocity of about 10^3 m/s /II.E.15/ was observed.

II.F Non-Stationary Ablation

Up to now we have treated the pellet ablation as a smooth process. This has been justified by the fact, that the time necessary for the cloud development is

more than one order of magnitude shorter than the ablation time which is of the order of half a millisecond. The observation of the D_α light during the pellet ablation, however, shows a different picture: The ablation rate changes strongly along the path of the pellet in the plasma; this modulation in the ablation is called "striations". Two effects are discussed in the literature to explain these striations: a) The striations are caused by an instability during the ablation, b) the ablation process is instantaneously "fed" by plasma energy nkT, which originates from closed magnetic surfaces. In this model it is considered, that close to rational values of the safety factor q(r), the energy reservoir is limited due to the resonant structure of the magnetic surface. When the pellet passes these positions, less heat flows to the pellet and therefore less particles are evaporated by the cloud. The strongest minima are generally observed, if the pellet passes the radius with "simplest" rational numbers q(r) = 1/1 and q(r) = 3/2. The method is applied for measuring the magnetic structure of the plasma by pellet-injection and will be resumed in section III.I.

In model a) /II.F.1/ the ablated atoms are ionized at a typical radius ρ_0. The attenuation of the incoming heat flux to the pellet at a given position depends on the ablation of a pellet in earlier times. The ablation is calculated to

$$\frac{dm}{dx} = f(x)\left(\frac{m(x)}{m_0}\right)^{2/3} \cdot \exp\left[\pi n(x)\int_0^{\rho_0} m'(x-\rho)\,\mathcal{G}(\rho)\,d\rho\right] \qquad \text{(II.6)}$$

In this expression f(x) is the ablation rate of an unshielded spherical pellet and is determined by the background plasma; $m(x)^{2/3}$ is the local pellet mass. The integral in the exponent gives the deposited mass per unit area at the position x; n(x) is the

inverse mass per unit area, which is attenuated by the energy flux along the field lines by 1/e and $g(\rho)$ is the radial cloud profile. An oscillating solution is obtained for an increasing cloud profile $g(\rho)$ and a bell shaped background plasma function f(x). A simulation yields an oscillation frequency in the ablating rate of about 80 kHz which corresponds to a striation distance of 1 cm. The 1 cm distance of the striations is - as perhaps expected - of the same order of magnitude as the cloud diameter. A picture of the observed time dependence and the calculated ones are shown in figs. II.7 a and b.

There are evidences that in tokamaks the simplest rational surfaces lead to observable striations, giving some support to model b. There are on the contrary also observations on experiments like the low shear stellarator /III.G.2/ where no low rational surfaces are present and striations are observed nevertheless. This implies that model b is not sufficient to explain the overall striation generation process.

III. Characteristics of Pellet Fuelled Discharges

The pellet injection changes several plasma properties. The obvious ones are the increase of the line averaged density and the decrease of the plasma temperature. Additionally the central density profile is steepened, the sawtooth activity is reduced or stopped, various internal plasma modes are excited and the central q-profile is altered. Several of these results are treated in review articles on the ASDEX tokamak by M. Kaufmann et al. /III.1 and III.2/; contributions of several other machines are collected in the IAEA-TECDOC-534 report /III.3/ and in a recent review paper by Chang /III.4/. Here these review articles are only summarized and

mainly newer results are discussed.

III.A The Profile Peaking

The ablation process starts at the periphery, where the pellet first touches the plasma, and continues until the pellet is fully consumed /III.A.1 - III.A.7/. In many cases this ablation is finished well before the pellet reaches the center of the plasma. In experiments like ASDEX (v_{pellet} = 600 m/s for centrifuge, 1000 m/s for gas gun) /III.1/ the penetration depth amounts to about 20 cm to 30 cm for Ohmic discharges at medium electron densities (e.g. 3 - 4 · 10^{19} m^{-3}). At very high initial electron densities (e.g. 6 · 10^{19} m^{-3}), i.e. at low initial plasma temperatures, the pellets can even pass entirely through the plasma. In this case the maximum ablation occurs near the center because the initial temperature is highest there. Very close to the axis, however, a minimum of the ablation is observed, because the energy reservoir on closed flux surfaces becomes infinitesimentally small there. In cases of additional heating, the plasma temperature near the boundary (i.e. in the gradient zone) is so high that the pellet gets already fully evaporated within 5 - 15, cm and the cloud of deposited atoms is concentrated near the periphery. In discharges with lower hybrid current drive /III.A.1/ the pellet can explode because the fast electrons penetrate the shielding cloud and deposit their energy inside the pellet (see also III.E).

A typical discharge with pellet injection is shown in fig. III.1. It is an example from the high-field ALCATOR C tokamak /III.A.2/ which was one of the earliest experiments showing the benefit of pellet injection. The top trace shows the electron density; the pellet injection is characterized by the sudden density rise at

about 380 ms. The increased density decays in 100 - 200 ms. Other traces in this figure will be discussed later.

The ablated plasma cloud in the periphery is quickly ionized and an inward drift sweeps the particles to the center; the time scale amounts to several milliseconds in ASDEX or some hundred milliseconds in JET (presently the largest tokamak) depending on the machine size, while the plasma density profile is steepened. The amplitude of this peaking strongly depends on the experimental conditions. It is most pronounced in Ohmic discharges with high electron densities. In strongly heated discharges a major profile peaking only occurs if the pellet reaches the $q = 1$ surface. For achieving this requirement at an experiment like JET, high pellet velocities become necessary. The development of the plasma density profile after the injection of a pellet in ASDEX is shown in fig. III.2. It is found that the density increases within a time span of about 17 ms. For the explanation of the peaking an inward pinch term has to be assumed, which is increased as compared to non-pellet-injection discharges at the same density (see III.C); the values of the transport coefficients governing the peaking evolution, namely the inward pinch (v) and the diffusion coefficient (D), are plotted at the bottom of the figure.

The pellet mode is of interest because the peaked density profile persists for some time and during this time several favorable properties like the plasma energy and the energy confinement time, are increased. This time duration depends again on the discharge parameters and on the size of the machine. In Ohmic discharges with low electron densities, the peaked plasma state is lost on a time scale less than or equal to the energy confinement time. The duration of the profile peaking - also with respect to the energy confinement time - increases with the line

averaged density. At the highest densities its duration amounts to several energy confinement times. Peaked profiles exist for medium size machines like ASDEX or TEXTOR 0.3 - 0.5 s, and for JET more than a second. During this peaking time the sawtooth activity of the plasma is in most cases suppressed.

III.B Plasma Energy and Confinement

In tokamaks and stellerators, the pellet ablation time is short compared to the energy confinement time. Therefore the radial distribution of pressure initially remains constant (neglecting the ionization and dissociation energy of the pellet); the heating energy of the ablated gas (ions) arising from the pellet is taken from the stored plasma energy. The plasma cools down rapidly during the pellet ablation. The temperature drop can be well over half the initial temperature without destroying the plasma. The temperature recovery time is faster than the density decay time. Therefore the plasma energy grows after the pellet has been injected if the initial density exceeds a certain value. An example of the temperature evolution due to the pellet injection is shown in fig. III.1, in the second trace. The other traces shown in fig. III.1 are the plasma current, the loop voltage, the Ohmic power, the β-value and the neutron yield. The Ohmic input power increases sharply after the pellet injection because of the increased plasma resistance due to the ablation cooling. The β value and especially the neutron yield show a remarkable maximum during the pellet mode.

In Ohmic discharges with pellet fuelling the energy content follows the linear ALCATOR scaling up to the highest densities. This means in other words that the energy confinement time τ_E increases without saturation up to very high densities,

in contrast to experiments without pellet injection. This scaling has been observed in all devices /III.A.1 - III.A.4/. Only at densities higher than $n_e \geq 6 \cdot 10^{14}$ cm^{-1} is a saturation found in Alcator. fig. III.3 shows an example of τ_E versus the line averaged density for Ohmic discharges on ALCATOR with gas fuelling and pellet fuelling /III.A.2/.

III.C Transport

The peaking of the plasma density profile is generally explained as a change in the transport coefficients for particles: the inward pinch $v_{in}(r) = (r/a)^{\sigma} \cdot v_{in}(a)$ and diffusion coefficient D. From the quasi steady state density profile the ratio v_{in}/D can be determined, and from the build-up time of the density profile the value of v_{in} can be estimated /III.C.1 - III.C.11/. In many experiments it is found that the diffusion coefficient is only poorly approximated by a radially constant value. A better approximation is a low central value and a higher boundary value. Several papers give more detailed distributions of the particle diffusion coefficient D or the heat conduction coefficients χ_e and/or χ_i. An example based on results from ASDEX is shown in fig. III.4. The χ_i value is close to the neoclassical Chang-Hinton value ξ_{CH}. Transport data given for ASDEX /III.C.3/ are D(0) = 0.05 m^2/s, D(2/3 a) = 0.1 m^2/s and v(2/3 a) = 0.5 m/s. The early ALCATOR experiments gave values of $<D>$ = 0.2 - 0.3 m^2/s /III.A.3/ and v = 1 m/s. Data for T-10 are D(0) = 0.2 - 0.3 m^2/s and v $\leq$ 10 m/s /III.C.9/. For JET the values are D = 0.08 m^2/s and v = 0.04 m/s /III.B.1/. These data from the different experiments give rather similar results; they were derived from the transport code TRANSP, developed in Princeton.

Very little has been published about the reason for the improved confinement using a self-consistent model. One exception is an attempt by A.A. Ware /III.C.12/. He subdivides the ion distribution function in a cold and a hot component. It is found that the collisions between the hot and cold ion species lead to a drag force such that the hot component flows preferentially towards the cold source. Ware uses this model for calculating the effects of recycling and of gas puffing, of pellet modes, of high confinement discharges (H-mode) and of the missing neoclassical peaking in normal discharges. The model explains some interesting features even though it cannot be expected that all these different problems can be resolved simultaneously.

III.D Pellet Injection during Additionally Heating

In early experiments it was difficult to reach good confinement in experiments with pellet injection and additional heating. The L-mode discharges showed a slight increase in τ_E /III.1/ when the pellets were injected during the L-mode phase. The H-mode confinement did not show a substantial improvement, e.g. in ASDEX. In other machines an improvement of the energy confinement was observed when injecting the pellets just before the switch-on of the neutral beams. Probably because of the relatively deep pellet penetration under this condition, the confinement could transiently be improved. Recently at JET /III.D.1 and III.D.2/ this mode of operation could be improved such that the good confinement mode persists for more than a second (PEP-mode; Pellet Enhanced Plasma-Mode), and during this time even an H-mode could be generated. To achieve the good confinement it was important to inject the pellet into the discharge before the first

sawtooth crash had developed. Fig. III.5 shows the density distribution of a PEP-H-mode discharge on JET. The good confinement regime is also here within the q = 1 surface.

III.E Combined Operation of Pellet Injection and Lower Hybrid Waves

If electromagnetic waves, so called lower hybrid waves, are be launched into a tokamak plasma, they either can heat the plasma, or more importantly, they can drive the discharge current of the tokamak (current drive). The difference between the two schemes is mostly established by the phasing of the launching antennae: unidirectional launching in the toroidal direction can transfer momentum to the electrons and lead to a current drive, while a radial launching heats the plasma. The current drive mode produces very energetic electrons (typically up to several hundred keV) and it is most efficient in low density plasmas. The zone of resonance can be shifted by adjusting the correct resonance condition.

Pellets injected into such plasmas experience strong ablation. The penetration depth as observed in ASDEX /III.E.1 -III.E.2/ is reduced from about 20 cm in an OH plasma to about 5 cm in a LH-current driven plasma of about the same density. When applying a series of pellets, the first ones stop at the boundary but the later ones penetrate deeper and deeper into the plasma until the Ohmic penetration depth is reached. This effect has been attributed to the destruction of the population of suprathermal electrons /III.A.1/.

Even though the pellets are predominantly evaporated near the boundary the plasma develops differently than with gas injection. The pellet injection favors again a density peaking while the gas puffing leads more to a flattening of the

density profile. The transport analysis shows a strong inward velocity of the plasma similar to that in the Ohmic case. In a similar way also the central diffusion coefficient drops by a factor of five. These features are reflected in the improvement of the energy confinement time, which can increase nearly to the Ohmic value after the injection of a series of pellets. The combination of pellet injection and LH current drive seems very promising for the next generation of tokamaks.

III.F Pellet Injection in ECRH Plasmas

Another heating mechanism consists of coupling high frequency waves, which resonate with the electrons (Electron Cyclotron Resonance Heating ECRH). Pellet injections into these ECR heated discharges have been performed at TFR /III.F.1 - III.F.2/. The observed ablation process exhibits some similarity with the one observed in LH current-driven plasmas: the pellets are quickly evaporated near the plasma boundary, probably due to the influence of suprathermal electrons. The ablation shows practically no striations in both cases. In TFR it was found that the ablation was independent of the position of the EC-resonance zone. An influence on the plasma performance due to the pellet injection was not reported.

III.G Pellet Injection in Reversed Field Pinches and Stellerators

Pellet injection experiments have not only been performed on tokamaks but also on reversed field pinches (RFP) and on stellerators. The control of the density seems to be very important for the RFP, because the phenomenon of 'density pumpout' during the RFP formation is often observed /III.G.1/. The pellet injection

leads to a fast and efficient fuelling for the relatively short RFP discharges (e.g. ZT-40M discharge time ≈ 35 ms). There are, however, some remarkable differences to pellet injection experiments in tokamaks. At first the ablation path is not nearly as straight as in other machines but strongly bent. In the case of toroidal field reversed pinch ZT-40M this deflection is typically downwards. By repositioning the injection angle the pellet could be better aimed to the center of the discharge. The deflection of the pellet path is attributed to an asymmetric flow of the power to the pellet; this asymmetry leads to an asymmetric evaporation and - by rocket effect - to the observed acceleration of the pellet perpendicular to the path.

The effect of the pellet injection on the plasma performance in the RFP is not as strong as in tokamaks. A plasma peaking is practically not observed. Shortly after the pellet ablation the profile becomes hollow and then recovers nearly to the old plasma shape at an enhanced line averaged density. A reason for this difference as compared to tokamaks may be the relatively short particle confinement time in the RFP which does not give enough time for the favorable profile effect to be established.

Concerning stellerators, pellet injection experiments have been performed on Heliotron and on Wendelstein 7-AS. Several plasma properties observed after pellet injection resemble those in tokamaks. In Heliotron /1.3,p. 73/ the profile peaks after the injection. The application of additional heating, both ECRH and neutral beams, deteriorates the confinement and the pellet does not penetrate deeply into the plasma. As a difference to the tokamak operation, it has been reported that the peaked density profile does not lead to a favorable energy confinement time. It is observed that peaked density profiles trigger internal modes which cause an

enhanced energy loss from the plasma. A rather favorable plasma operation is found when applying a combination of gas puffing and pellet injection.

On Wendelstein /III.G.2/ also a deterioration of the energy confinement is reported to occur just after the injection of the pellet. This effect is pronounced in ECR generated discharges and in Ohmic discharges. Only in cases of neutral beam heating does the enhanced plasma target density after pellet injection lead to a favorable plasma condition with enhanced energy content. A combination of neutral beams and ECR deteriorates again the plasma properties. Surprisingly, the ablation pattern in Wendelstein has shown striations similar to those observed in tokamaks /see § II.F/. The striations were not expected because Wendelstein is characterized by its low shear. Therefore, the existing theories of the formation of striations, which were based on the changing energy reservoirs for the ablation connected with rational flux surfaces, cannot be applied here.

III.H Sawteeth

Sawtooth activity is observed in most tokamak discharges. It is a prominent feature in the time dependence of the central temperature and of the central density. As the name 'sawtooth' suggests, the signals increase rather linearly over some time and then drop rapidly to their minimum values. Afterwards the increase starts again. The time span of a sawtooth increases with the size of the machine, with the electron density and under additionally-heated plasma conditions. A necessary condition for the occurrence of sawteeth is most likely the existence of a $q = 1$ surface in the plasma. The sawtooth activity is probably an instability at or inside this surface. The sawtooth activity leads to an increased expulsion of

particles and energy out of the plasma.

After a pellet injection the sawtooth activity of Ohmically heated plasmas is normally reduced or it can even stop for some time. This trend increases with increasing density. The pellet-induced reduction of density decay time and improvement of energy confinement time mentioned above just follow from the improved transport properties. After some time the peaked density profile has smeared out and the sawtooth activity starts again, as shown in fig. III.6 measured on TEXTOR.

III.I Mode Excitation and 'Snakes'

Connected with the injection of pellets into the plasma, several types of plasma oscillations have been observed. In ALCATOR C a $n=1$, $m=1$ mode is triggered immediately after the ablation of the pellet /III.I.1/. From electron temperature and soft X-ray measurements it has been concluded that the mode is governed by density fluctuations and not by temperature fluctuations. The density fluctuation amounts to about 3% and the modes rotate poloidally in the electron diamagnetic drift direction. The wave type is of acoustic character because the frequency of the oscillations vary with the atomic mass of the pellet (hydrogen or deuterium). The maximum of the mode is at $r = 5$ cm, well outside the $q = 1$ surface ($r_{q=1} = 3.5$ cm). The fact that the observed mode structure does not correspond to the resonant plasma surfaces imposes a difficulty on the interpretation of the current profile determination from the location of the modes /see III.J.1/. Also other modes like $m=1$, $m=2$ or $m=3$ are observed in ALCATOR C /III.I.1/, but not as well localized as the $n=1$, $m=1$ type.

Additionally to the oscillations immediately following the pellet injection, at TEXTOR a mode has been found starting with a time delay of about 10 ms and lasting for another 10 ms /III.I.2/. This mode is shown in fig. III.7. The frequency is typically 0.7 - 2 kHz and is between that of ALCATOR C (about 5 kHz) and JET / JT-60 (0.03 - 1 kHz). Like in ALCATOR C the perturbation is mainly in the density and practically not in the temperature.

In ASDEX, the sawtooth activity is reduced by the first pellet. The quiescent period lasts for about 100 ms /III.C.6/. Thereafter moderate $m = 1$, $n = 1$ oscillations gradually develop and are damped out about 200 ms later. The MHD activity has no detrimental effect on the profile peaking.

Ballooning-type modes /III.I.3/ have been made responsible for a fast cold front propagation preceeding the pellet in TFR. The radial progression velocities of these modes amount to about 1000 m/s and a turbulent zone up to 10 cm preceeding the pellet is observed.

A similar cold front was found in the JIPP-TIIU tokamak /III.I.4/. Also here the cold front precedes the injected pellet on its way into the plasma. The front velocity is different in the plasma outside the $q = 1$ surface from that inside the $q = 1$ surface. On the outside it is lower, but still faster than the pellet velocity. The $q = 1$ surface was identified by the sawtooth inversion radius. Discharges without sawteeth exhibit the lower front velocity all over the plasma.

A more persistent perturbation than the oscillations treated so far has been observed at JET and was called a 'snake' /III.I.5 and III.I.6/. A snake is characterized by a density perturbation winding like a snake around the central part of the plasma as shown in Fig. III.8. In most cases the winding is around the $q = 1$

surface but there have also been described snake structures at the $q = 3/2$ surface. The snake is clearly seen in the pictures of an X-ray camera at JET. It has a lifetime of 1-2 seconds and survives without major distortions the sawtooth crashes. The snake is sometimes destroyed in soft disruptions or in a very large sawtooth collapse. It is generally assumed that the snake is a large island structure inside the plasma. It occurs when the ablation of the pellet extends well into the $q = 1$ area. To achieve this it is advantageous to inject a combination of two or more pellets. The first pellet(s) cool the plasma so that the successive pellets penetrate deeper into the plasma. The pellet particles ablated near the $q = 1$ surface may be confined and form the island. The density within the snake can be up to twice that of the surrounding plasma, although the number of particles in the snake is only about 1% of the injected pellet particles. Like other islands, the snake normally rotates around the central plasma, but like locked modes, it can also stay at a fixed position inside the torus.

III.J Current Distribution:

The current distribution is one of the most important characteristics of a tokamak discharge. It determines to a large extent whether the discharge is stable or not, if internal crashes (sawteeth) occur, and where internal plasma modes develop. In the last chapters the importance of the current distribution was implicitely discussed several times. The current distribution, however, is not easily measured. Methods are the determination of the Faraday rotation of a probing laser beam (e.g. HCN interferometer - polarimeter), measurements of the Zeeman splitting of injected neutral beams (lithium or hydrogen isotopes) or the evaluation

of the position of resonant internal modes (e.g. sawtooth inversion radius). Another, also rather indirect, method of determining the plasma current bases on the analysis of of the jxB force establishing the radial plasma pressure distribution. The analysis is mainly performed by plasma-equilibria codes.

The pellets contribute also to the plasma current measurement in a twofold way by a) the modulation of the ablatant gas during the pellet injection (striations) and b) due to the alignment of these striations along the magnetic field. The modulation (a) is probably linked with island structures inside the plasma. In /III.J.4 - III.J.6/ it is assumed that the ablation process is fed from closed surfaces in the plasma. Non rational surfaces are the largest energy reservoirs for the pellet ablation, while islands near rational q-surfaces are small reservoirs. The alignment (b) shows immediately the inclination of the magnetic fields and with known toroidal magnetic field, the poloidal component, i.e. also the electrical current, can be evaluated.

The H_α signal arising from the ablation of a pellet injected into JET, the q-profile near $q = 1$ and the current distribution are shown in fig. III.9. From the time dependence of the H_α-signal, it is deduced that the region around the $q = 1$ surface has a low shear. This low shear is attributed to the formation of an island. The flattening of the current density at the plasma inside is obvious from the lower trace.

On JT-60 /III.J.2/ the current distribution is derived from plasma pressure and on JET /III.J.3/ both from the pressure and the location of the oscillations. The results indicate that the central current density of the discharge increases after the pellet injection. According to the plasma pressure rise, the increase is mostly

attributed to the bootstrap current. The discharges exhibit a typical sawtooth behavior before the pellet injection and a stop of the sawteeth due to the pellet injection. The analysis showed a central current increase in both cases. At JT-60, however, the current profile deformation is not sufficient to lift the central q-value above one, while in the case of JET the central value is lifted such that the q-profile stays above one everywhere. The q-value is not increasing monotonically in the radial direction, but has a maximum on the axis. If the result of JT-60 is correct, the stop of the sawteeth is not caused by the q distribution. It should be mentioned, however, that the measurements of the current profile are rather indirect so that the error margin is probably still large.

III.K Impurities

Concerning impurities, various kinds of investigations are performed in pellet-fuelled discharges. There is at first a dilution of the plasma due to pellet injection, there is the impurity accumulation under some pellet mode conditions, there is the active impurity injection by impurity doping of pellets and there are finally the impurity pellets which have quite different properties from hydrogen isotope pellets.

The injection of hydrogen isotope pellets does not only lead to an improvement of the plasma confinement, but also cleans transiently the plasma /III.K.3/. The clean plasma state, however, is not permanent; already during the density peaking phase it disappears. The additional heating immediately following the pellet injection can increase the impurity level further.

More details of an impurity accumulation is shown in fig. III.10, obtained at

JET /III.K.1/. The accumulation of light- and medium-Z impurities is not observed in all cases but predominantly in cases with strong density peaking and a suppression of the sawteeth. The improved confinement in fig. III.10 lasts for about 3 s as can be seen from the density trace. Also here the injection of pellets leads at first to a cleaner plasma, but about 1 s after the pellet injection the NiXXVI intensity starts to rise and reaches a value several times higher than without pellet injection. This accumulation is expected from the neoclassical theory. After the onset of the sawtooth activity the nickel concentration is reduced again. With respect to this impurity accumulation the good-confinement pellet mode is similar to other good-confinement modes like the H-mode or the ASDEX counter neutral beam injection mode /III.K.2/.

By carefully controlling the freezing temperature during the pellet formation, hydrogen isotope pellets with tracer impurities can be produced. In ASDEX /III.K.4/ neon has been used in such a mixture. By this procedure the neon can quickly be brought into the plasma and, from the time sequence of the different ionization states and the subsequent decay, the transport coefficients in the plasma for the medium-Z material can be deduced. An example for this measurement is given in fig. III.11. The transport coefficients obtained in this way agree well, within the experimental errors, with those derived from the other transport calculations.

Impurity pellets have been formed by solid materials like plastic (for carbon) or steel. These impurities can be used for fuelling (LiH) or for transport studies, but up to now have mainly been used for ablation studies /III.K.5/. The interaction of these pellets with the plasma is quite different from that of the hydrogen isotope pellets. The reason for the difference is based on the much higher evaporation

temperature of the impurity pellets. They are nearly insensitive to fast particles which destroy the hydrogen pellets, and thus penetrate deeper into the plasma. Therefore they have been used e.g. in discharges with lower hybrid current drive /III.K.6/. From visible Bremsstrahlung it was found that the peaking in the two types of discharges is very different. On the TEXT tokamak /III.K.5/ the striations from different impurity pellets were analyzed. It is consistent to assume that the striations there are formed at rational q-surfaces and the position of these magnetic surfaces can be derived. fig. 12 shows an example of this striation measurement with a strong modulation depth at $q=2$ and $q=1$.

IV.A Application of Pellet Injection in the Fusion Reactor

For a future reactor-like device like ITER tokamak different aspects of the pellet dominated discharges are of interest /IV.1-2/. One scenario of the discharge initiation is the application of lower hybrid waves, similar as shown in § III.5, for ramping up the plasma current. This wave coupling to the plasma for current drive is efficient only at low plasma densities. After having reached the full plasma current, pellet injection can help to reach quickly the final density.

When a sufficiently high discharge current is reached, the plasma can be fuelled either by gas injection or by pellet injection. The injection of burn gas has a low efficiency and the gas is preferably swept into the divertor from where it is pumped away again. This scenario would therefore require unnecessary large amounts of circulating tritium. For the pellet injection, both shallow and deep fuelling are foreseen. For the deep fuelling, pellets with a velocity of 5 km/s or more are required. The deep fuelling leads to a good central confinement with a

peaked density profile. This profile is favorable to ignite the central plasma and therefore up to 50 high speed injections are planned just after the ramp up phase.

During the burn phase of ITER an H-mode type discharge is favored. The discharge shows a rather flat density and pressure distribution with a pedestal at the plasma edge; the temperature distribution is somewhat more peaked and also has a pedestal. The energy confinement is improved by a factor of 1.5 - 3 as compared to a normal L - mode discharge. The main reason for the choice of an H-mode discharge type is the improved energy confinement of the plasma. This choice of the plasma pressure distribution is also close to the optimal β - profile for the Troyon limit. If pellets with high velocities are injected deeply into the plasma, the density profile will peak. The peaked high confinement mode is not desired during the burn phase of the discharge because the burn rate of the D/T fuel is too high, and the power load to the walls may become intolerably high. Therefore the pellet injection with shallow fuelling possibly together with gas puffing is foreseen for the ITER quasi steady burn phase. In the optimal case, the pellet ablation occurs just past the separatrix. In this zone a part of the newly introduced fuel will diffuse into the core and replenish the consumed fuel; another part will be swept to the divertor, together with the helium ash coming from the core, and finally will be pumped away. The dilution of the ash will help to prevent a back-diffusion of the ash to the core which otherwise would poison the fuel.

IV.B Pellet Ablation and Disruptions

Between pellet injection and disruptions two connections can be established. The first one is the density limit disruption during the pellet injection. In general it

is observed that the line averaged density limit with pellet injection is higher than in gas fuelled discharges. The reason for this difference may be related to the special mechanism of density limit disruptions and the special feature of density peaking during pellet injections. The density limit in tokamaks is determined by the temperature of the plasma edge /IV.3/, which in turn depends on the edge density and on the heating power. If the temperature at the edge drops below a critical value, islands develop at the $q = 2$ surface and grow until the discharge collapses. Due to the strong peaking of the density profile after a pellet injection, the density at which this collapse occurs is increased.

The second connection between pellet injections and disruptions is, to our knowledge, not yet treated in the literature. During disruptions extremely high energy fluxes occur on the limiters or on the divertor strike zones. This power flux leads to a sudden evaporation of the limiter / divertor material and a subsequent shielding against the incoming power /IV.4/. For the ITER divertor strike plates calculations predict a shielding cloud with densities of the order of 10^{18} - 10^{19} cm^{-3}. These densities are well comparable to the densities in the pellet ablation cloud and theories of the cloud shielding - especially of impurity pellets - would most likely be applicable for this case.

Acknowledgement

I would like to express my gratitude to K. Büchl and W. Hofer for many hints and discussions and M. Chatelier and J. Schou for their comments and for carefully reading the manuscript.

References

I. Introduction

I.1 B.S. Gottfried, C.D. Lee, K.J. Bell, 'The Leidenfrost Phenomenon', Int. J. Heat Mass Transfer, 9, (1966) 1167

I.2 Y.Y. Hsu, 'Review of Film Boiling at Cryogenic Temperatures', Adv. Cryogenic Eng., 17, (1972) 361

II. Pellet Ablation

II.A.1 R.D. Birkhoff, 'Passage of Fast Electrons Through Matter' in S. Flügge, Handbuch Physik, Springer Verlag Berlin 34 (1958) 53

II.A.2 Dalgarno, 'Range and Energy Loss' in D.R. Bates, Atomic and Molecular Processes, Academic Press, NY (1962) 623

II.A.3 K. Büchl, 'Messung von Energieverlusten von Elektronen' Diplomarbeit Juni 1959, TU-München

II.A.4 S. Valkealahti, J. Schou, H. Sørensen, R.M. Nieminen, 'Ranges and Stopping Power of keV Electrons in Solid Hydrogen', Nucl. Instr. Meth. in Phys. Res., B34 (1988) 321

II.A.5 J. Schou, H. Sørensen, P.Børgesen, 'Measurement of Electron-Induced Emission of Condensed Gases', Nucl. Instr. Meth. in Phys. Res. B5 (1984) 44

II.A.6 B. Stenum, J. Schou, O. Ellegard, H. Sørensen et al., 'Sputtering of Solid Targets by keV Hydrogen Ions', Phys. Rev. Lett. 67 (1991) 2842

II.A.7 P. Børgesen, H. Sørensen, 'Stopping of Light Ions in Solid Hydrogens', Nucl. Instr. Methods in Phys. Res. 200 (1982) 571

II.A.8 H. Sørensen, J. Schou, 'On the Emission of Electrons from Solid H_2 and D_2', J. Appl. Phys., 53 (1982) 5230

II.A.9 J. Schou, B. Stenum, H. Sørensen, K.V. Weisberg, 'Radiation in the Wavelength120-900 nm from keV Electron ombardment of Solid Hydrogens', Nucl. Fus. 31 (1991) 589

II.A.10 J.A. Forrest, R.L. Brooks, J.L. Hunt et al., 'Continuum Emission from Irradiated Solid Deuterium', Phys. Rev. B 46 (1992) 13820

II.B Ablation Modelling

II.B.1 P.B. Parks, R.J. Turnbull, C.A. Foster, 'A Model for the Ablation Rate of a Solid Hydrogen Pellet in a Plasma', Nucl. Fus., 17 (1977) 539

II.B.2 P.B. Parks, R.J. Turnbull, 'Effects of Transsonic Flow in the Ablation Cloud on the Lifetime of a Solid Hydrogen Pellet', Phys. Fluids 21 (1978) 1735

II.B.3 S.L. Milora, C.. Foster, 'A Revised Neutral Gas Shielding Model for Pellet-Plasma Interactions', IEEE Trans. Plasma Sci., PS-6 (1978) 578

II.B.4 S.L. Milora, 'Review of Pellet Fuelling', J. Nucl. Energy 1 (1981) 15

II.B.5 C.T. Chang, 'Vaporization Mode and State of the Ablatant of a Deuterium Pellet', Phys Fluids, 26 (1983) 805

II.B.6 C.T. Chang, L. Thomsen 'On the Correlation Between the H_α-Line Emission Rate and the Ablation Rate of a Hydrogen Pellet in Tokamak Discharges' Nucl. Fus. 24 (1984) 697

II.B.7 C.T. Chang, L.W. Jørgensen, L.W. Nielsen, L.L. Lengyel, 'The Feasability of Pellet Re-Fuelling of a Fusion Reactor', Nucl. Fus. 20 (1980) 859

II.B.8 W.A. Houlberg, S.L. Milora, S.E. Attenberger, 'Neutral Plasma Shielding Model for Pellet Ablation' Nucl. Fus. 28 (1988) 595

II.B.9 L.L. Lengyel, 'Expansion of Dense Particle Clouds in Magnetically Confined Plasmas', Phys. Fluids 31 (1988) 1577

II.B.10 L.L. Lengyel, 'Pellet-Plasma Interaction', Nucl. Fus. 29 (1989) 37

II.B.11 L.L. Lengyel, G.G. Zavala, O. Karsaun et al., 'Evaluation of Pellet Clouds and Cloud Structures', Nucl. Fus. 31 (1991) 1107

II.B.12 L.L. Lengyel, 'Evolution of Particle Clouds Around Ablating Pellets in Magnetically Confined Hot Plasmas', Report IPP 5/41 Garching, Aug. 1991

II.B.13 L.L. Lengyel, 'Assessment of Pellet Injection for NET', Report IPP 1/232, Garching, Sept. 1984

II.B.14 M. Salvat, 'Analytical Solutions for Spherically Expanding Pellet Matter' Report IPP 4/186, Garching, Apr. 1980

II.B.15 Y. Nakamura, H. Nishihara, M. Wakatani, 'An Analysis of the Ablation Rate for Solid Pellets', Nucl. Fus. 26 (1986) 907

II.B.16 B.V. Kuteev, A.P. Umov, L.D. Tsendin, 'Kinetic Model for the Evaporation of Hydrogen Pellets', Sov. J. Plasma Phys., 11 (1984) 236

II.B.17 G.G. Zavala, T. Kammash, 'Nonspherical Pellet Ablation', Fus, Techn. 6 (1984) 30

II.B.18 Y. Nakamura, K. Kiji. M. Wakatani et al., 'Ablation Model Including the Particle Energy Distribution Function and Pellet Ablation by Hot Ions in Heliotron E', Nucl. Fus. 32 (1992) 2229

II.B.19 P.B. Parks, 'Electric Field and Current Distribution Near the Ablation Cloud of a Pellet Injected into a Plasma', Nucl. Fus. 32 (1992) 2137

II.B.20 S.K. Ho, L.J. Perkins, 'Pellet Ablation Modelling in Reactor-Grade Plasmas', Fus. Techn. 14 (1988) 1314

II.C Ablation Rate

II.C.1 W.A. Houlberg, S.E. Attenberger, L.R. Baylor et al., 'Pellet Penetration Experiments on JET', Nucl. Fus. 32 (1992) 1951

II.D Penetration Depth of Pellet

II.D.1 M.J. Dunning, F.J. Mayer, Z. Kammash, 'Time Dependent Simulation of Pellet Evaporation in Tokamak Plasmas', Nucl. Fus., 30 (1990) 919

II.E Experimental Observations of the Ablating Pellet

II.E.1 G.L Schmidt, D. Bartlett, L. Baylor et al., 'Fuelling of JET Limiter and X-Point Plasma by Deuterium Pellet Injection' Controlled Fusion and Plasma Physics (Proc. 19th Eur. Conf., Innsbruck 1992) Vol. 16C, p. II-255 (1992)

II.E.2 L.R. Baylor, G.L. Schmidt, W.A. Houlberg et al., 'Pellet Fuelling Deposition Measurements on JET and TFTR', Nucl. Fus. 32 (1992) 2177

II.E.3 K. Büchl, G.C. Vlases, W. Sandmann, R. Lang, 'Correlation of Pellet Penetration Depths on ASDEX for Ohmic and Auxiliary Heated Discharges', Nucl. Fus., 27 (1987) 1939

II.E.4 R. Loch, W. Sandmann, K. Büchl et al., 'Scaling of Experimentally Determined Penetration Depths on ASDEX', Controlled Fusion and Plasma Physics (Proc. 17th Eur. Conf., Amsterdam 1990) Vol. 14B, p. I-235 (1990)

II.E.5 L.L. Lengyel, K. Büchl, W. Sandmann, 'Pellet Penetration in ASDEX: A Comparison of Results Computed by the ORNL Ablation Model with Measured Data', Controlled Fusion and Plasma Physics (Proc. 16th Eur. Conf., Venice 1989) Vol. 13 p. I-179 (1989)

II.E.6 S.L. Milora, G.L. Schmidt, W.A. Houlberg et al., 'Pellet Injection into PDX Diverted Tokamak Plasmas', Nucl. Fus. 22 (1982) 1263

II.E.7 B.V. Kuteev, V. Sergeev, A.P. Umov, 'Evaporation Rate and MHD Perturbations During Pellet Injection into the T-10 Tokamak', Sov. J. Plasma Phys. 14 (1988) 1

II.E.8 D.H. McNeill, G.J. Greene, J.D. Newburger el al., 'Measurements of Plasma Parameters in the Luminous Regions of Pellets Injected into the Tokamaks', Controlled Fusion and Plasma Physics (Proc. 14th Eur. Conf., Madrid 1987) Vol. 11D, p. I-209 (1987)

II.E.9 D.H. McNeill, G.J. Green, D.D. Schuresko, 'Parameters of the Luminous Region Surrounding Deuterium Pellets', Phys. Rev. Lett., 55 (1985) 1398

II.E.10 R.D. Dust, W.L. Rowan, M.E. Austin et al., 'Experimental Observations of the Dynamics of Pellet Ablation on the Texas Experimental Tokamak (TEXT)', Nucl. Fus., 30 (1990) 3

II.E.11 D.H. McNeill, 'H-Alpha Photon Yield in Fuelling of Tokamaks', J. Nucl. Mater. 162 - 164 (1989) 476

II.E.12 TFR Group, 'Pellet Injection Experiments on the TFR Tokamak', Nucl. Fus., 27 (1987) 1975

II.E.13 B. Pegourié, J.L. Bruneau, J.M. Picchiottino, 'Parallel Expansion of the Ablation Cloud During Pellet Injection in Tore Supra', Controlled Fusion and Plasma Physics (Proc. 18th Eur. Conf., Berlin 1991) Vol. 15C, p. I-313 (1991)

II.E.14 B. Pegourié, J.-M. Picchiottino, H.-W. Drawin et. al., 'Pellet Ablation Studies on Tore Supra', Nucl. Fus. 33 (1993) 591

II.E.15 S.M. Egorov, V.A. Galkin, V.G. Kapralov et al.,'Pellet Ablation Study in T-10 using a Photographic Technique', Proc. 13th Int. Conf. Plasma Phys. Contr. Fus. Research, IAEA-CN-53/A-VII-13, Washington, p. 599 (1990)

II.F.1 J. Neuhauser, R. Wunderlich, 'A Model for Periodic Pellet Ablation in Toroidal Confinement Experiments', Report IPP 5/30, Garching, Nov. 1989

III. Characteristics of Pellet Fuelled Discharges

III.1 M. Kaufmann, 'Review of Pellet Fuelling', Plasma Phys. Contr. Fus., 28, 1341-1352, (1986)

III.2 M. Kaufmann, K. Büchl, G. Fussmann et al., 'Pellet Injection with Improved Confinement in ASDEX', Nucl. Fus., 28, 827 - 848 (1988)

III.3 IAEA-TECDOC-534, 'Pellet Injection and Toroidal Confinement', Proc. Techn. Committee Meeting, IAEA, Vienna, 1989

III.4 C.T. Chang, 'Pellet-Plasma Interactions in Tokamaks' Physics Reports, 206 (1991) 143

III.A The Profile Peaking

III.A.1 F.X. Söldner, V. Mertens, R. Bartiromo et al., 'Combined Operation of Pellet Injection and Lower Hybrid Current Drive in ASDEX', Plasma Physics and Controlled Fusion, 33 (1991) 405

III.A.2 M. Greenwald, D. Gwinn, S. Milora et al., 'Energy Confinement of High-Density Pellet-Fuelled Plasmas in the ALCATOR C Tokamak', Phys. Rev. Lett., 53, 352-355, (1984)

III.A.3 M. Greenwald, J. Parker, M. Bensen et al., 'Hydrogen Pellet Injection in ALCATOR C', Controlled Fusion and Plasma Physics (Proc. 11th Eur. Conf., Aachen 1983) Vol. 7D, p. 7-10 (1983)

III.A.4 A.D. Cheetham, D.J. Campbell, A. Gondhalekar et al., 'Profile Effects with Pellet Fuelling of JET', Controlled Fusion and Plasma Physics (Proc. 14th Eur. Conf., Madrid 1987) Vol. 11D, p. 205-208 (1987)

III.A.5 K. Shimuzu, R. Yoshino, Y. Kamada and T. Hiramaya, 'Simulation Study of Pellet Fuelled Plasmas in JT-60', Nucl. Fus., 31, 2097-2106, (1991)

III.A.6 L.A. Charlton, L.R. Baylor, A. Edwards el al., 'MHD Analysis of Peaked Pressure Profiles Produced by Pellet Injection in JET', JET report JET-P(90)65

III.A.7 H. Drawin and TFR-Group, ' Hydrogen and Deuterium Pellet Injection into Ohmically and Additionally ECR-Heated FR Plasmas', Controlled Fusion and Plasma Physics (Proc. 14th Eur. Conf., Madrid 1987) Vol. 11D, p. 213 - 216 (1987)

III.B Plasma Energy

III.B.1 S.L. Milora, D.V. Bartlett, L.R. Baylor et.al., 'Summary of Energy and Particle Confinement in Pellet-Fuelled Auxiliary-Heated Discharges in JET', Controlled Fusion and Plasma Physics (Proc. 16th Eur. Conf., Venice 1989) Vol. 13B, p. 91 - 94 (1989)

III.B.2 M.Kaufmann, W. Sandman, M. Bessenrodt-Weberpals et al., 'Electron Temperature Profiles in Discharges with Pellet Injection and in Other Mode Discharges', Controlled Fusion and Plasma Physics (Proc. 16th Eur. Conf., Venice 1989) Vol. 13B, p. 47 - 50 (1989)

III.B.3 S.L. Milora, G.L. Schmidt, V. Arunasalam et al., 'Confinement of High-Density Pellet Fuelled Discharges in TFTR', Plasma Phys. Contr. Fus., 28, 1435-1439 (1986)

III.B.4 A. Stäbler, H. Niedermeyer, R. Loch et al., 'Densits Limit in ASDEX Discharges with Peaked Density Profiles' Controlled Fusion and Plasma Physics (Proc. 16th Eur. Conf., Venice 1989) Vol. 13B, p. 23 - 30 (1989)

III.B.5 Y. Kamada, N. Hosogane, R. Yoshino et al, 'Study of the Density Limit with Pellet Fuelling in JT-60', Nucl. Fus. 31 (1991) 1827

III.C Transport

III.C.1 O. Gruber, M. Kaufmann, K. Lackner et al., 'Comparison of Confinement in Hydrogen versus Deuterium in Multi-Pellet Fuelled OH Discharges in ASDEX' (Proc. 15th Eur. Conf., Dubrovnik 1988) Vol. 12B, p. 27 - 30 (1988)

III.C.2 O. Gruber, H.U. Fahrenbach, O. Gehre et al., 'Auxiliary Heated Multipellet-Fuelled Discharges in ASDEX and Influence of Density Profile shape on Confinement', Plasma Physics and Controlled Fusion, 30 (1988) 1611

III.C.3 V. Mertens, K. Büchl, O. Gruber et al., 'Particle Transport and Sawtooth Activity in Pellet-Fuelled ASDEX L-Mode Plasmas', Controlled Fusion and Plasma Physics (Proc. 16th Eur. Conf., Venice 1989) Vol. 13B, p. 183 - 186 (1989)

III.C.4 V. Mertens, 'Electron Density Transport in JET after Single Pellet Injection', JET-IR(88)06

III.C.5 A. Gondhalekar, A.D. Cheetham, J.C.M. de Haas et al., 'Simultanous Measurements of Elektron Thermal and Particle Transport in JET', Plasma Physics and Controlled Fusion, 31 (1989) 805

III.C.6 V. Mertens, M. Kaufmann, R. Lang et al., 'Electron Particle Transport Properties of Sawtooth-Free Pellet-Fuelled ASDEX Discharges', IPP-Report: IPP 1/258, (1991)

III.C.7 V. Mertens, M. Bessemrodt-Weberpals, G. Dodel et al., 'Physics of Enhanced Confinement with Peaked and Broad Density Profiles', Plasma Physics and Controlled Fusion, 32 (1990) 965

III.C.8 G. Vlases, K. Büchl and D. Campbell, 'Studies of Tokamak Transport based on Pellet Injection', Controlled Fusion and Plasma Physics (Proc. 11th Eur. Conf., Aachen 1983) Vol. 7D, p. 127-130 (1983)

III.C.9 V.G. Kapralov, B.V. Kuteev, M.A. Parshin et al., ' Plasma Perturbation during Hydrogen Pellet Injection on T-10', Controlled Fusion and Plasma Physics (Proc. 18th Eur. Conf., Berlin 1989) Vol. 15C, p. 345 - 348 (1991)

III.C.10 G. Haas, M. Kaufmann, R.S. Lang et al., Recycling Studies in the ASDEX Divertor with Pellet or Gas Puff Refuelling', Journal Nucl. Mater., 145 - 147, 519 - 522 (1987)

III.C.11 V. Mertens, M. Kaufmann, K. Büchl et al., 'Pellet Injection with Improved Confinement in ASDEX', Controlled Fusion and Plasma Physics (Proc. 14th Eur. Conf., Madrid 1987) Vol. 11D, p. 33 - 36 (1987)

III.C.12 A.A. Ware, 'The Rapid Inward Diffusion of Cold Ions in Tokamaks and their Effect on Ion Transport', DOE/ET-53088-405 IFSR #405 (1989)

III.D Pellet Injection during Additional Heating

III.D.1 P. Kupschus, A. Cheetham, B. Denne et. al., 'Multi Pellet Injection in JET', Controlled Fusion and Plasma Physics (Proc. 15th Eur. Conf., Dubrovnik 1988) Vol. 12B, p. 143 - 146 (1988)

III.D.2 B.J.D. Tubbing, B. Balet, D.V. Bartlett et al., 'H-Mode Confinement in JET with Enhanced Performance by Pellet Peaked Density Profiles', Nucl. Fus., 31, 839 - 850 (1991)

III.E Combined Operation of Pellet Injection and Lower Hybrid Waves

III.E.1 F.X. Söldner et al., Proc. 13th International Conf. on Plasma Physics and Controlled Nuclear Fusion Research, Washington, IAEA-CN-53/E-1-1 (1990)

III.E.2 K. Büchl et al., Nucl. Fusion, 27 (1987) 1939

III.F Pellet Injection in ECRH Plasmas

III.F.1 H.W. Drawin and TFR-Group, 'Hydrogen and Deuterium Pellet Injection into Ohmically and Additionally ECR-Heated Plasmas', Controlled Fusion and Plasma Physics (Proc. 14th Eur. Conf., Madrid 1987) Vol. 11D, p. 213 - 216 (1987)

III.F.2 H.W. Drawin, A. Geraud, 'Pellet Injection into Ohmically Heated and Electron Cyclotron Resonance Heated Tokamak Plasmas', Nucl. Fus., 29 (1989) 1681

III.G Pellet Injection in Reversed Field Pinches and in Stellerators

III.G.1 G.A. Wurden, P.G. Weber, R.G. Watt et al., Nucl. Fusion, 27 (1987) 857

III.G.2 K.P. Büchl, W VII-A team, NI-Team, ECRH-Team, 'Pellet Ablation in the W VII-A Stellerator', IPP-Report, IPP 1/238 (1986)

III.H Sawtooth

III.I Mode Excitation and 'Snakes'

III.I.1 J. Parker, M. Greenwald, R. Petrasso et al., 'Observation of m=1, n=1 Oscillations Following the Injection of a Fuel Pellet into the ALCATOR C Tokamak, Nucl. Fusion, 27, 853 - 856 (1987)

III.I.2 K.N. Sato, S. Kogoshi, H. Akiyama et al., 'Studies on Fast Oscillations and on Particle Transport during Sawtooth Crashes in Pellet

Injected TEXTOR Plasmas', Controlled Fusion and Plasma Physics (Proc. 18th Eur. Conf., Berlin 1989) Vol. 15C, p. 333 - 336 (1991)

III.I.3 X. Garbet, L. Laurent, F. Mourgues, J.-P. Roubin, A. Samain, 'Turbulence Propagation during Pellet Injection', Controlled Fusion and Plasma Physics (Proc. 16th Eur. Conf., Venice 1989) Vol. 13B, p. 299 - 302 (1989)

III.I.4 M. Sakamoto, K.N. Sato, Y. Ogawa et al., 'Fast Cooling Phenomena with Ice Pellet Injection in JIPP T-IIU Tokamak', Plasma Physics and Controlled Fusion, 33 (1991) 583

III.I.5 A. Weller, A.D. Cheetham, A.W. Edwards et al., 'Persistent Density Perturbations at Rational q Surfaces Following Pellet Injection in the JET European Torus', Phys. Rev. Lett., 59, 2303 -2306 (1987)

III.I.6 A.W. Edwards, D. Campbell, A. Cheetham et al., 'Measurements of SNAKES Following Multiple Pellet Fuelling of JET', Controlled Fusion and Plasma Physics (Proc. 15th Eur. Conf., Dubrovnik 1988) Vol. 12B, p. 143 - 342 - 345 (1988)

III.J Current Distribution:

III.J.1 H. Soltwisch, Plasma Physics and Controlled Fusion, 'Current Density Measurements in Tokamak Devices', 34 1669 - 1698 (1992)

III.J.2 R. Yoshino, 'Current Profile Modification in JT-60 Pellet Injection Experiments', Nucl. Fusion, 29, 2231 - 2234 (1989)

III.J.3 M. Hugon, B.Ph. van Milligen, P. Smeulders et al., 'Shear Reversal and MHD Activity during Pellet Enhanced Performance Plasmas in JET', Nucl. Fusion, 32 (1992) 33

III.J.4 B. Pégourié, M.A. Dubois, 'Diagnostic of the Current Density Profile in the Vicinity of q = 1: The H_α Emission of Ablated Pellets', Nucl. Fus. 30 (1990) 1575 - 1584

III.J.5 M.A. Dubois, R. Sabot, B. Pegourié et al., 'Determination of the Safety Factor Profile in Tore Supra from the Largest Striations observed during Pellet Ablation', Nucl. Fus. 32 (1992) 1935

III.J.6 D.K. Mansfield, A.T. Ramsey, M.G. Bell et al., 'Observation of Rational Magnetic Surfaces in TFTR Using the Emission From Ablating Deuterium Pellets', Nucl. Fus. Lett. 33 (1993) 150

III.K Impurities

III.K.1 K. Behringer, B. Denne, A. Edwards et al., 'Impurity Transport during H-Mode, Monster Sawteeth and after Pellet Injection', Controlled Fusion and Plasma Physics (Proc. 15th Eur. Conf., Dubrovnik 1988) Vol. 12B, p. 338 - 341 (1988)

III.K.2 K.H. Steuer, H. Röhr, G. Fussmann et al., 'Impurity Accumulation and Z_{eff} Profiles in ASDEX High Confinement Regimes, Controlled Fusion and Plasma Physics (Proc. 16th Eur. Conf., Venice 1989) Vol. 13B, p. 191 - 194 (1989)

III.K.3 P.D. Morgan, A. Boileau, M.J. Forrest et al., 'Studies of Visible Impurity Radiation from JET Plasmas during Heating and Fuelling Experiments', Controlled Fusion and Plasma Physics (Proc. 16th Eur. Conf., Venice 1989) Vol. 13B, p. 95 - 98 (1989)

III.K.4 K. Behringer, K. Büchl, 'Impurity Transport Studies in ASDEX by Means of Neon-Seeded Pellets', IPP report, IPP III/137, (1988)

III.K.5 S.C. McCool, G.G. Castle, B.A. Smith et al., 'Impurity Pellet Experiments in TEXT', Controlled Fusion and Plasma Physics (Proc. 18th Eur. Conf., Berlin 1989) Vol. 15C, p. 325 - 328 (1991)

III.K.6 S. Morita, E. Kawatoh, K. Ohkubo et al., 'Impurity Pellet Injection into Current Driven Plasmas of the JIPP T-IIU Tokamak', Nucl. Fus., 30, 938-944

IV.A Application of Pellet Injection for the fusion reactor

IV.1 F. Engelmann and NET team, 'Prospectives of Pellet Injection in NET-Like Devices', Comments Plasma Phys. Controlled Fusion, 12, 293 - 304 (1989)

IV.2 K. Tomabechi, J.R. Gilleland, Yu.A. Sokolov, R. Toschi and ITER team, 'ITER Conceptual Design', Nucl. Fus., 31, 1135 - 1224 (1991)

IV.3 M. Bessenrodt-Weberpals, K. McCormick, F.X. Söldner et al., Nucl. Fusion 31 (1991) 155

IV.4 J.G. Gilligan, M. Bourham, O. Hankins et al., 'Vapor Shield Protection on Plasma Facing Components under Incident High Heat Flux', presented at PSI 1992 and to be published in J. Nucl. Mater.

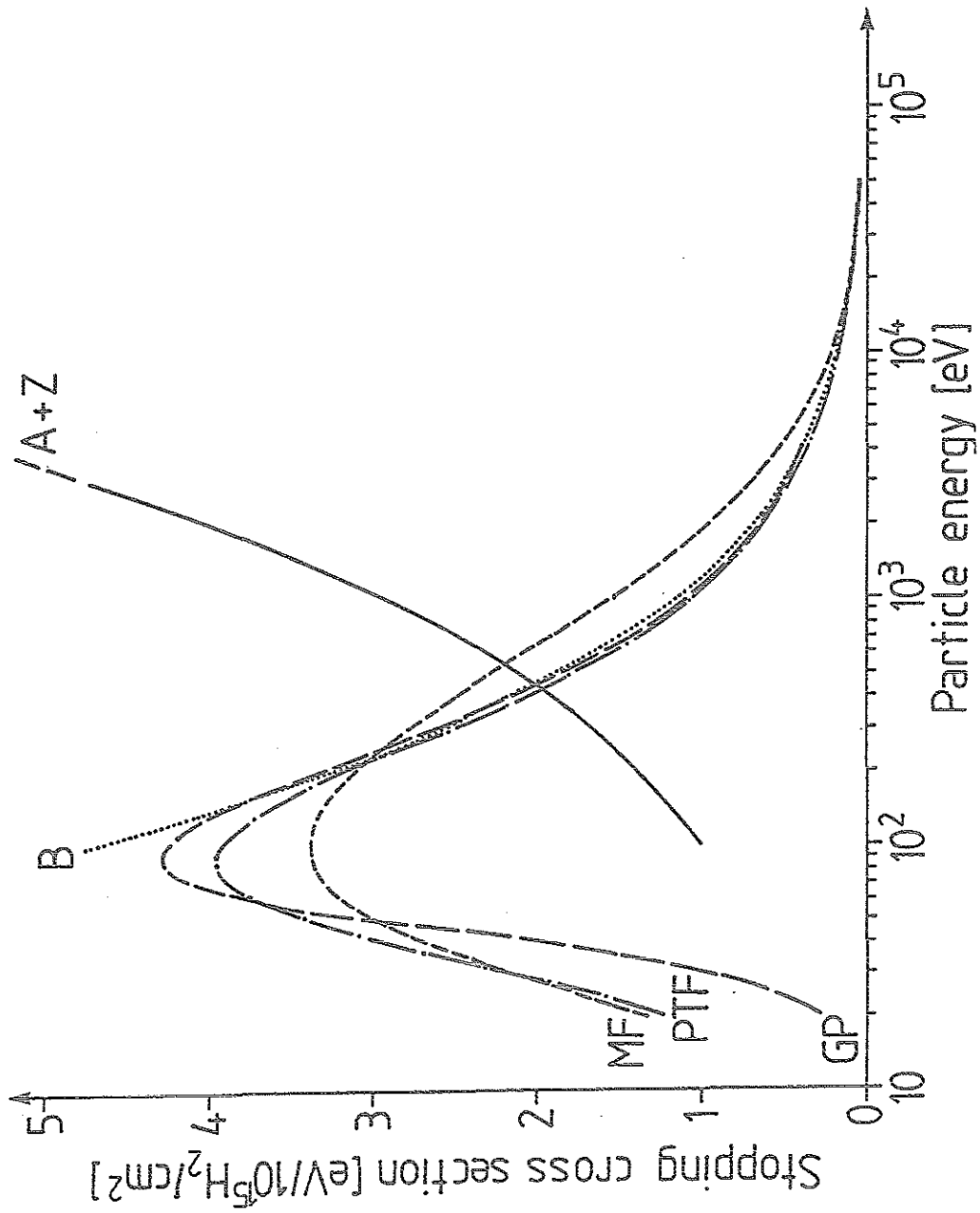

Fig. II.1 Stopping cross section for electrons and ions as a function of energy. (Obtained from J. Schou)

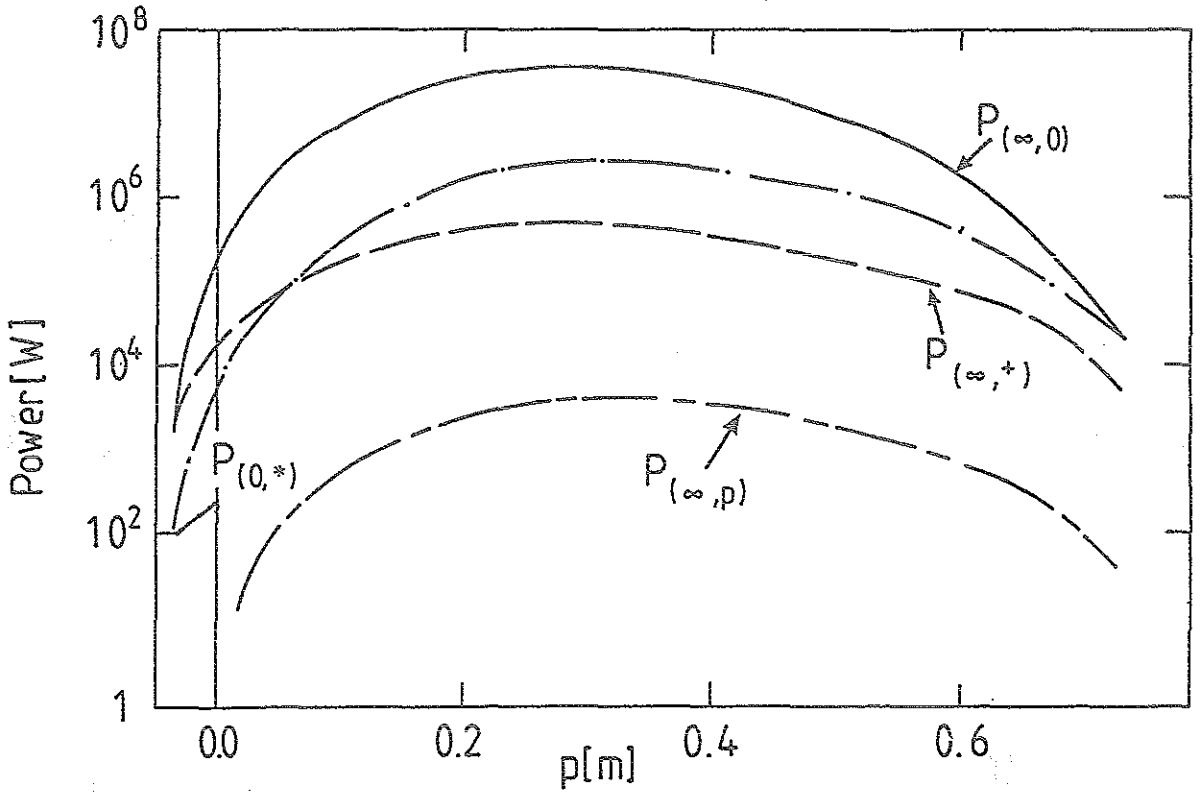

Fig. II.2: Power flux to different shells of the ablating pellet for an example of Tore Supra /II.E.14/: The top curve is the flux falling to the outer shell of ionized ablated cloud. The next two curves represent the flux of thermal and high energy electrons to the interface between ionized and neutral cloud and the lower curve is the flux to the pellet. The coordinate ρ is the normalized radial position of the injected pellet. The curves are plotted in semi-logarithmic scale.

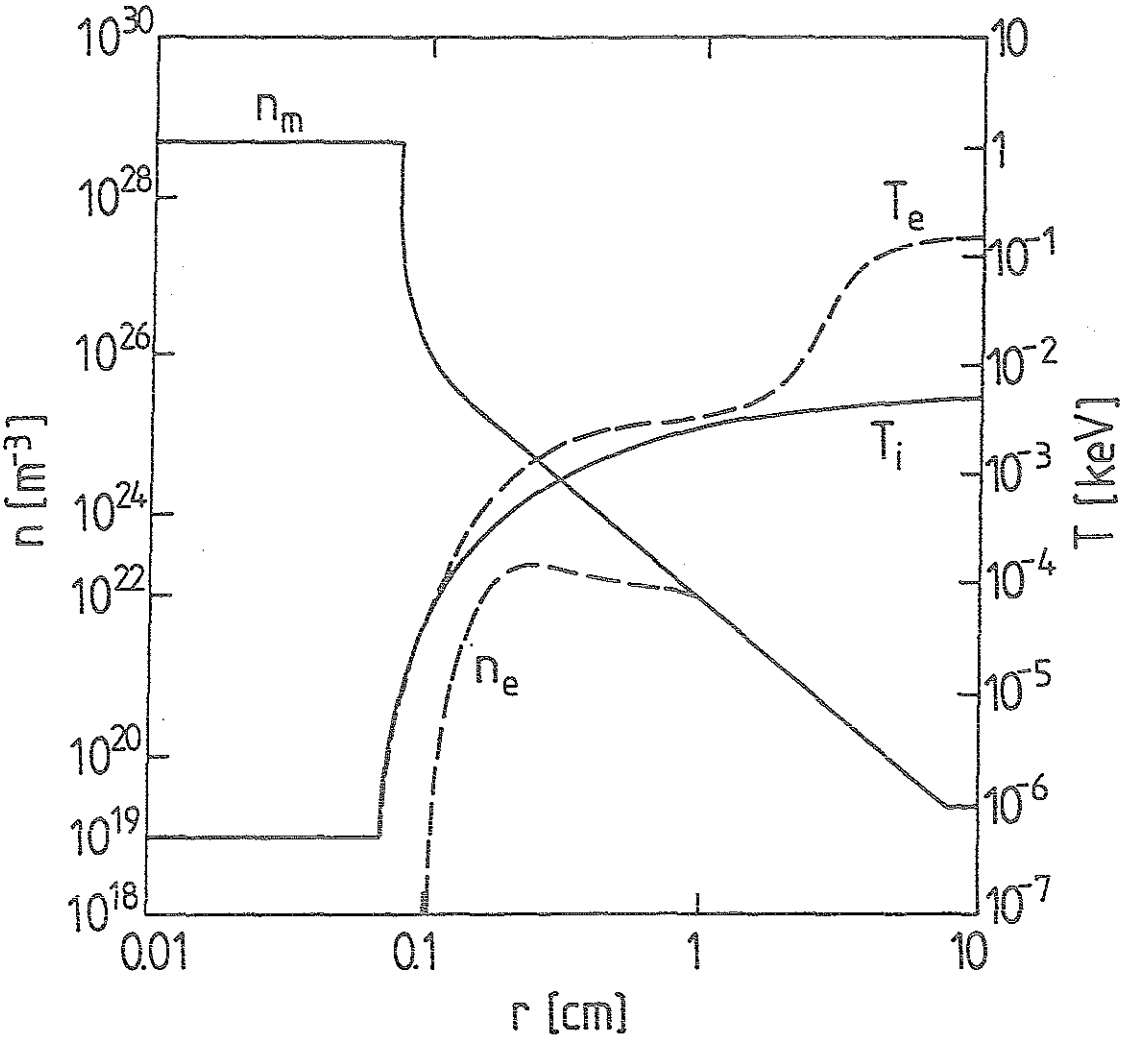

Fig. II.3 Simulated electron (n_e) and specific mass ($n_m = \rho/m_i$) densities and electron (T_e) and ion (T_i) temperatures of the ablatant as a function of teh radius at 25 μs after injection into a discharge /II.D.1/. The solid pellet extends over the radius n_m = const.

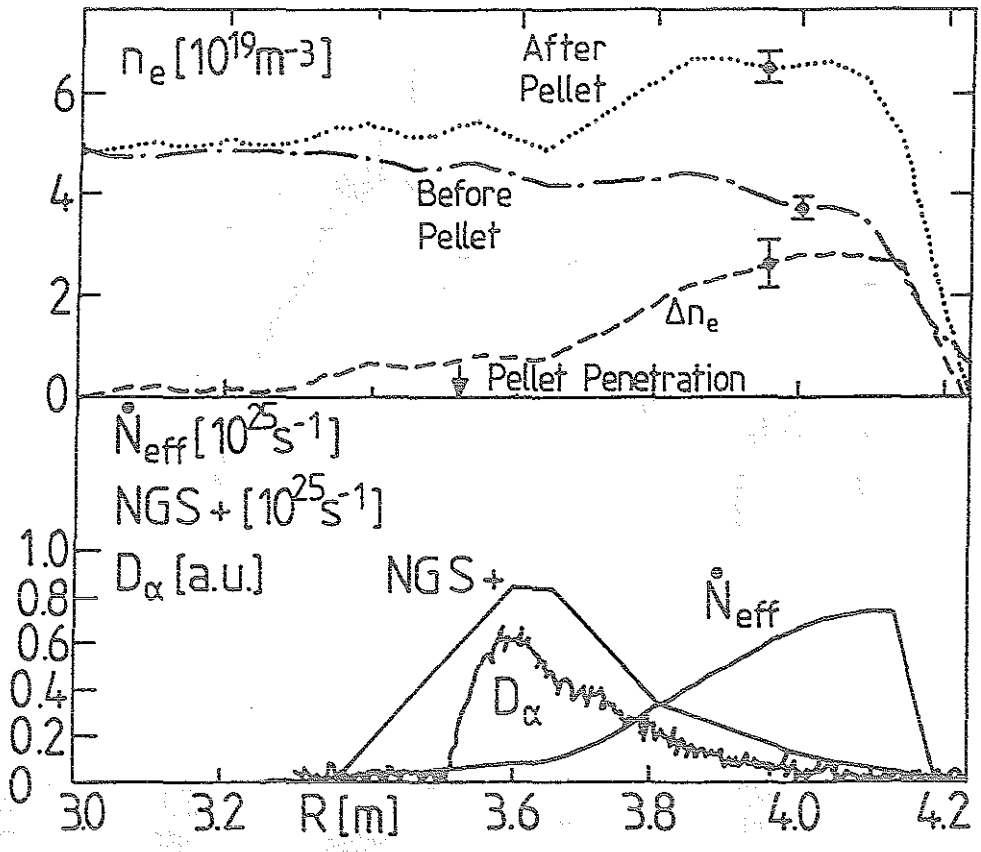

Fig. II.4 Mass deposition immediately after pellet injection. Top: Radial density profile before and after pellet injection and the difference between these values Δn_e. Bottom: D_α emission from ablation according to the NGS-model and Δn_e converted to dN_{eff}/dt /II.E.1/

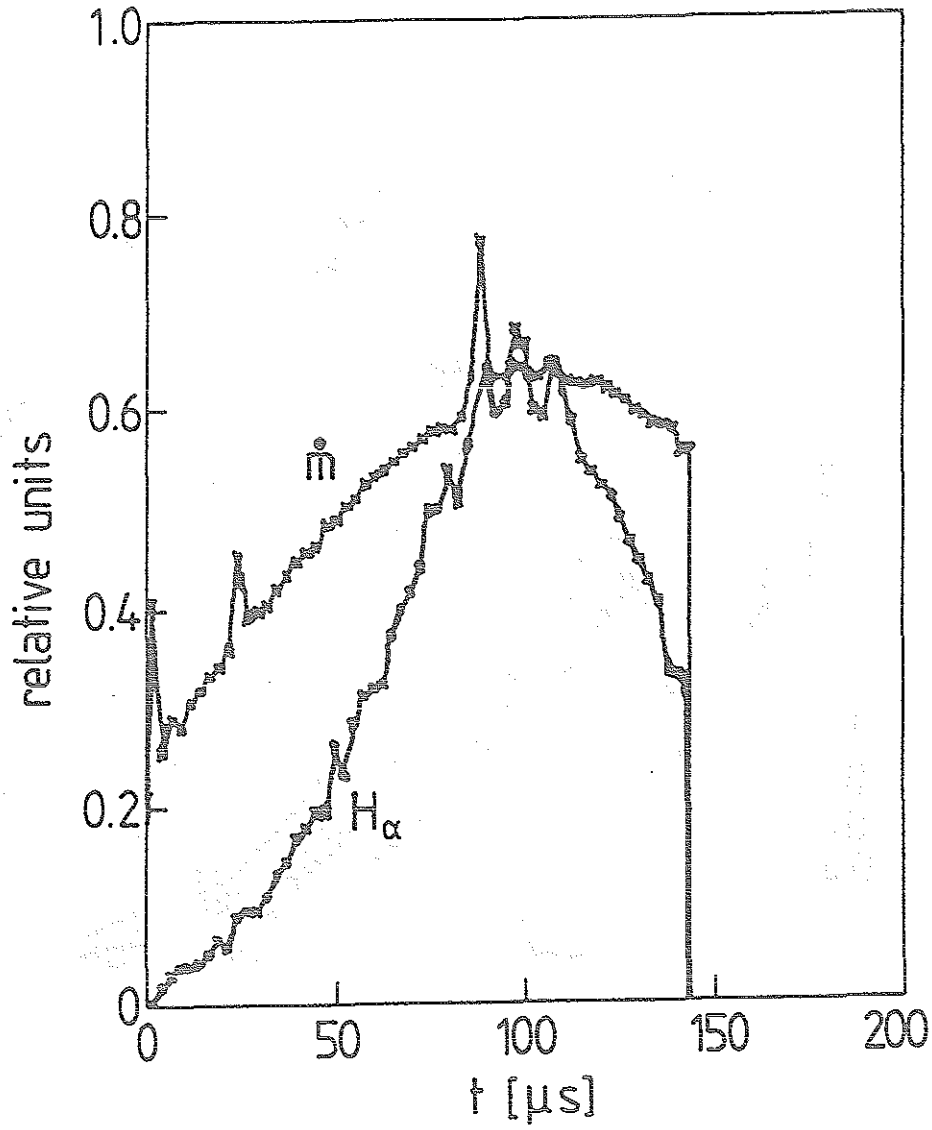

Fig. II.5 The calculated H_α luminosity profile and the mass ablation rate at the pellet surface /II.D.1/.

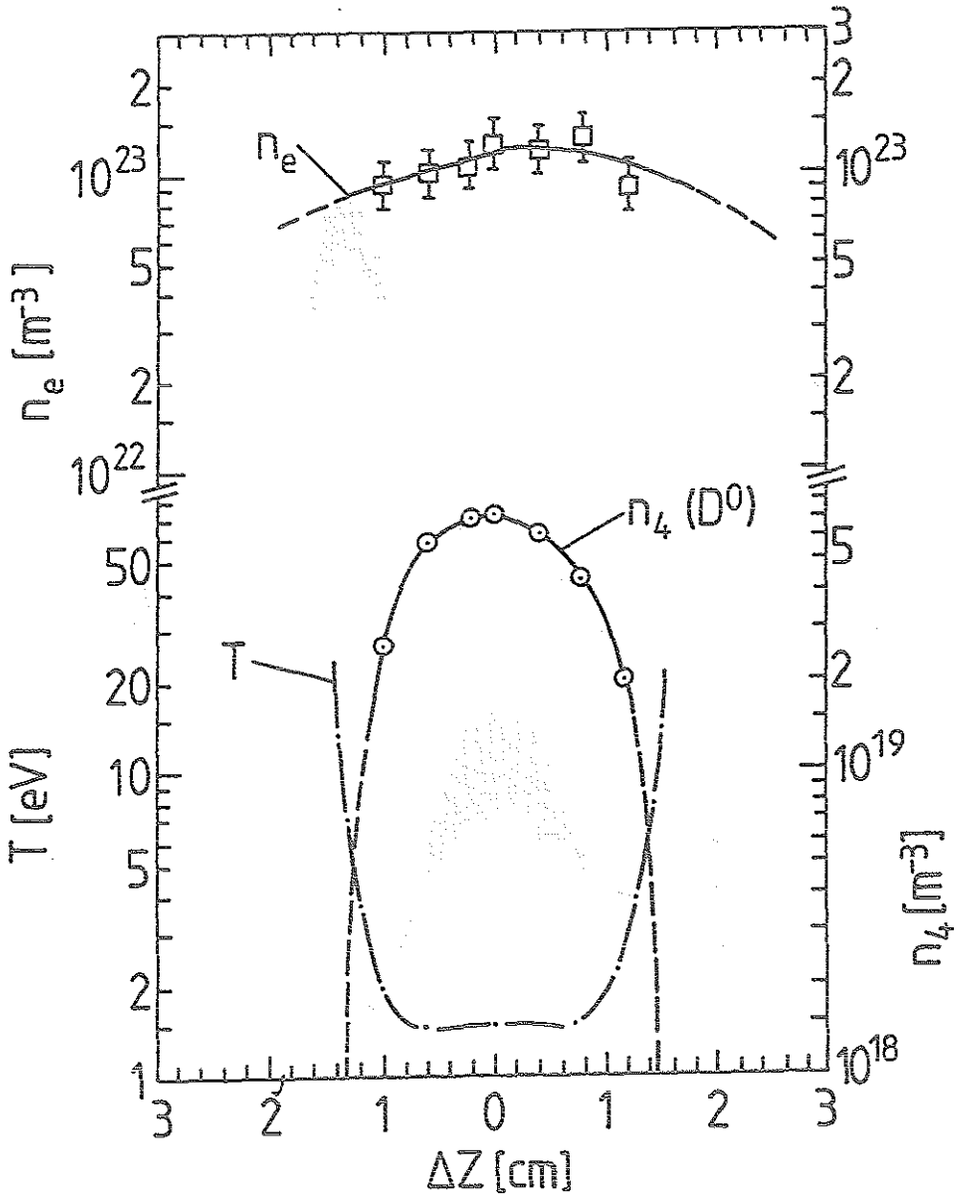

Fig. II.6 Electron density, $n_e(z)$, neutral atom density, $n_4(z)$, and temperature, $T(z)$, along a striation /II.E.12/.

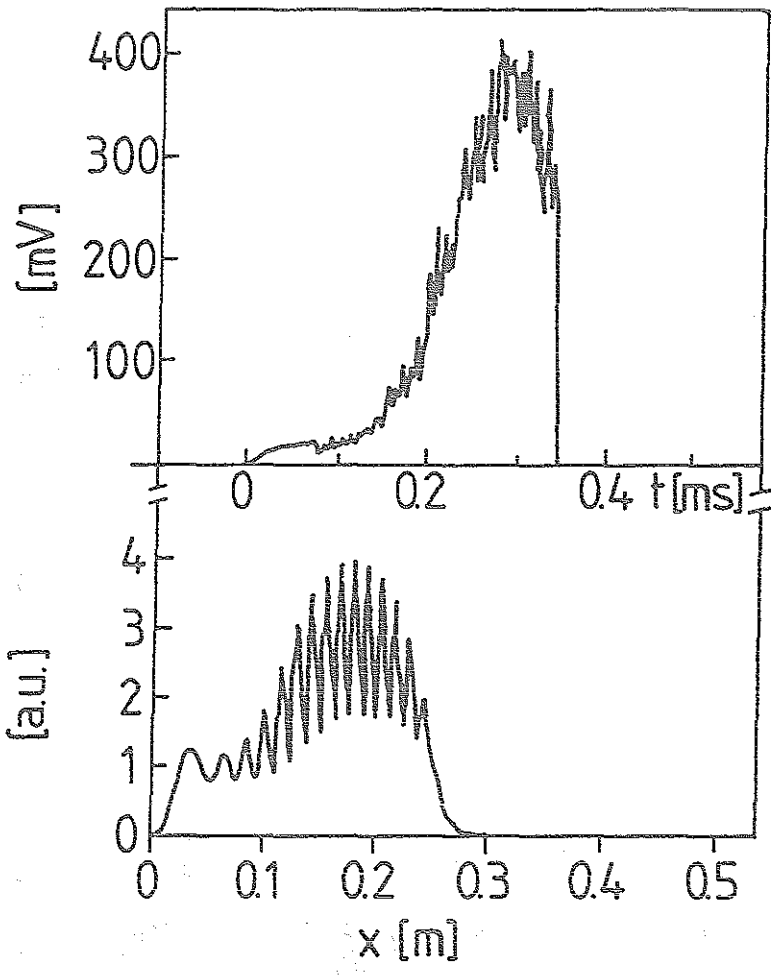

Fig. II.7 Top: Modulations of the D_α-emission during a pellet passage in TEXTOR. Bottom: Numerically calculated modulation of the pellet ablation according to Neuhauser /II.F.1/

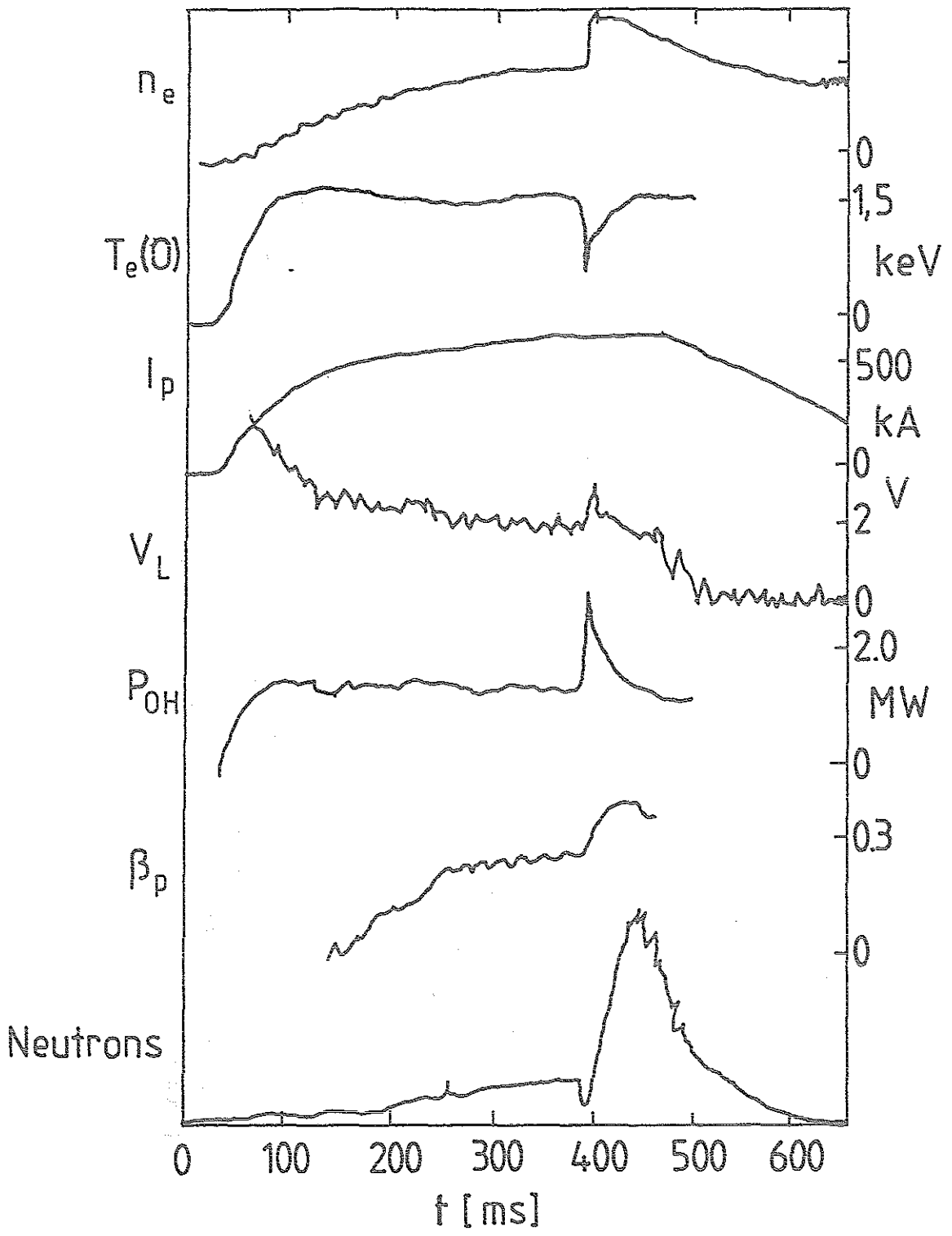

Fig. III.1 Series of signals taken from ALCATOR /III.A.2/. From top to bottom the signals are: Line averaged density, central electron temperature, plasma current, loop voltage, ohmic power input, β_{pol} and the neutron yield.

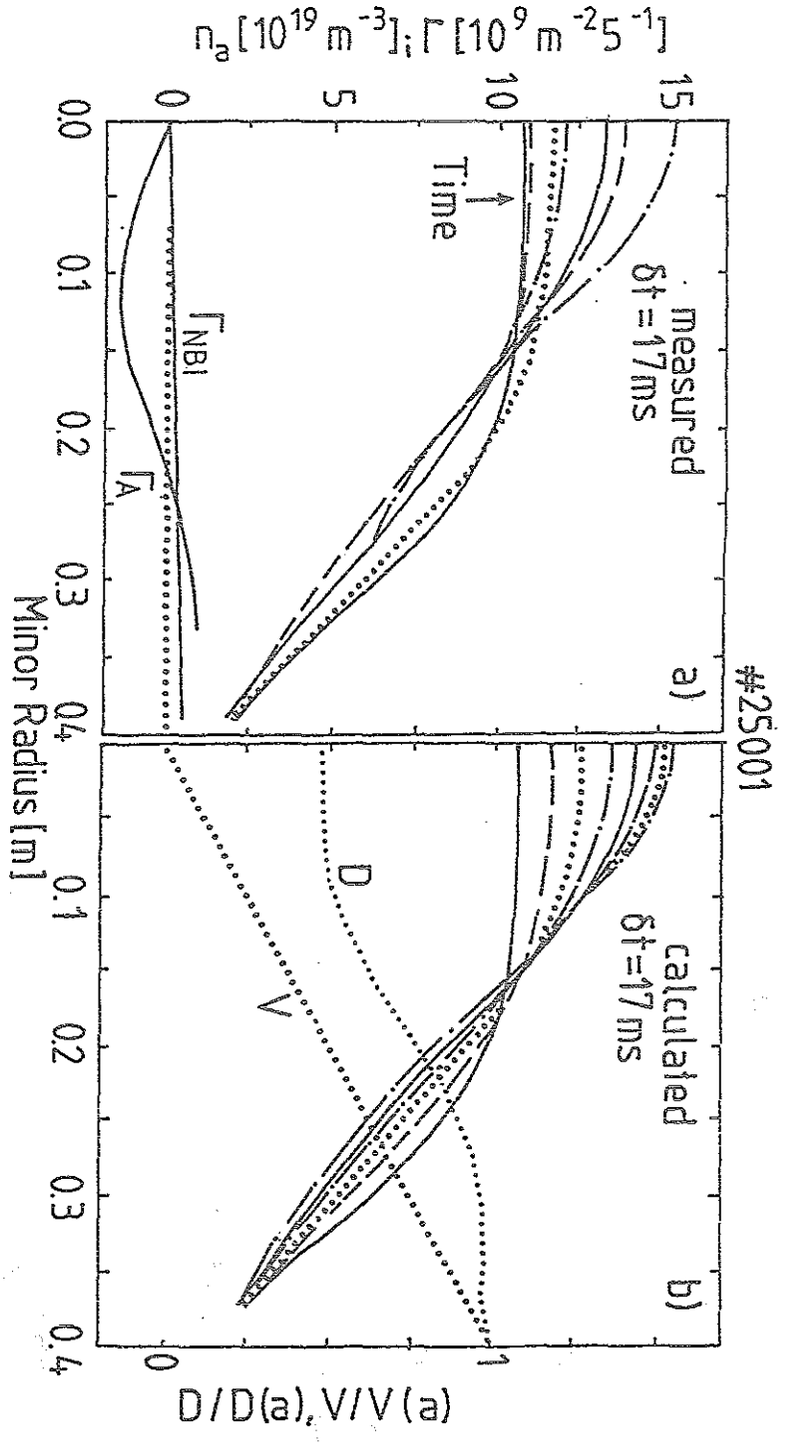

Fig. III.2 Density evolution a) measured by Thomson scattering and b) calculated after pellet injection. The time between each profile is 17 ms. Transport coefficients for particles are shown on the bottom. The data are taken from ASDEX /III.C.6/.

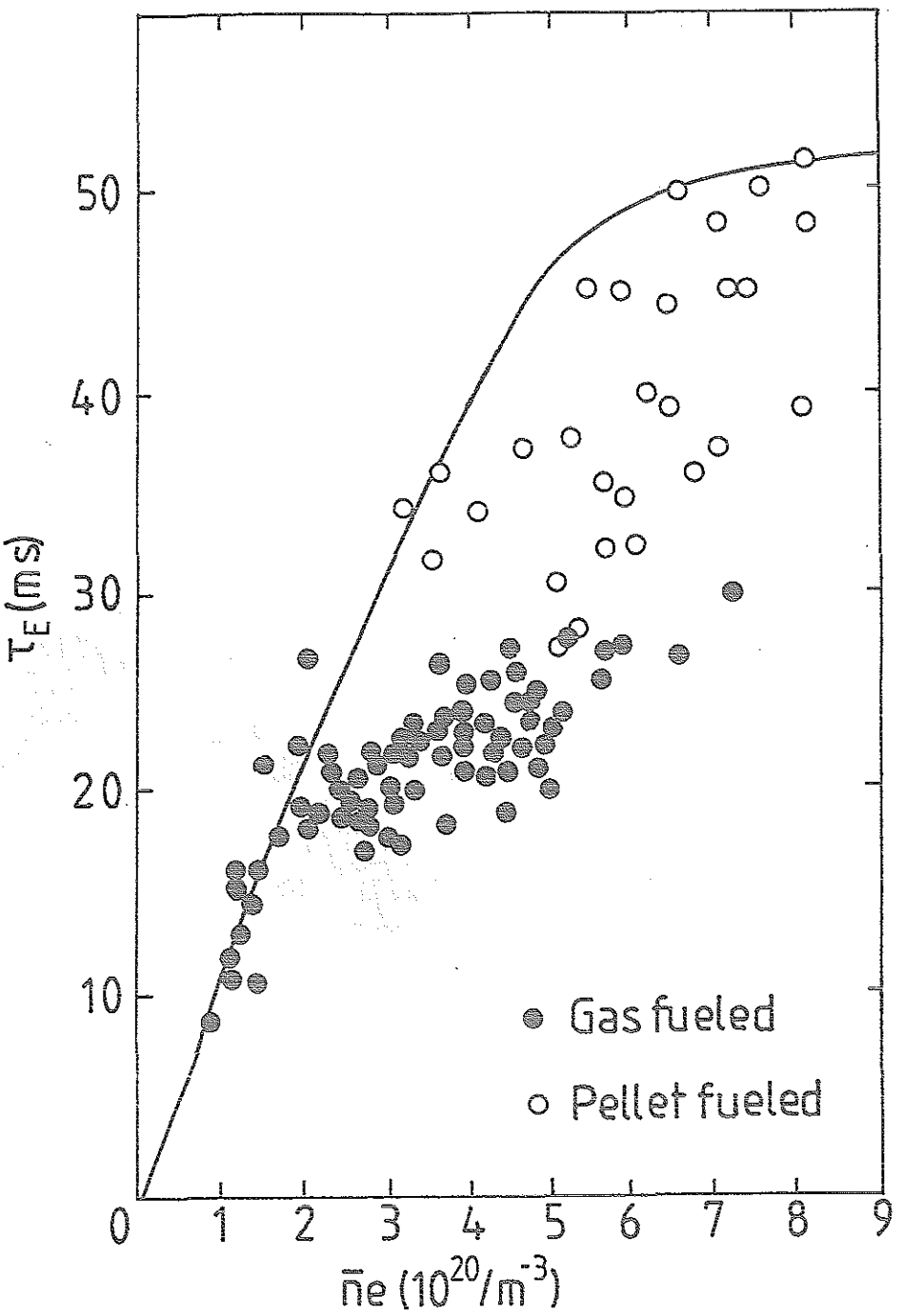

Fig. III.3 Energy confinement time measured on ALCATOR C /III.A.2/.

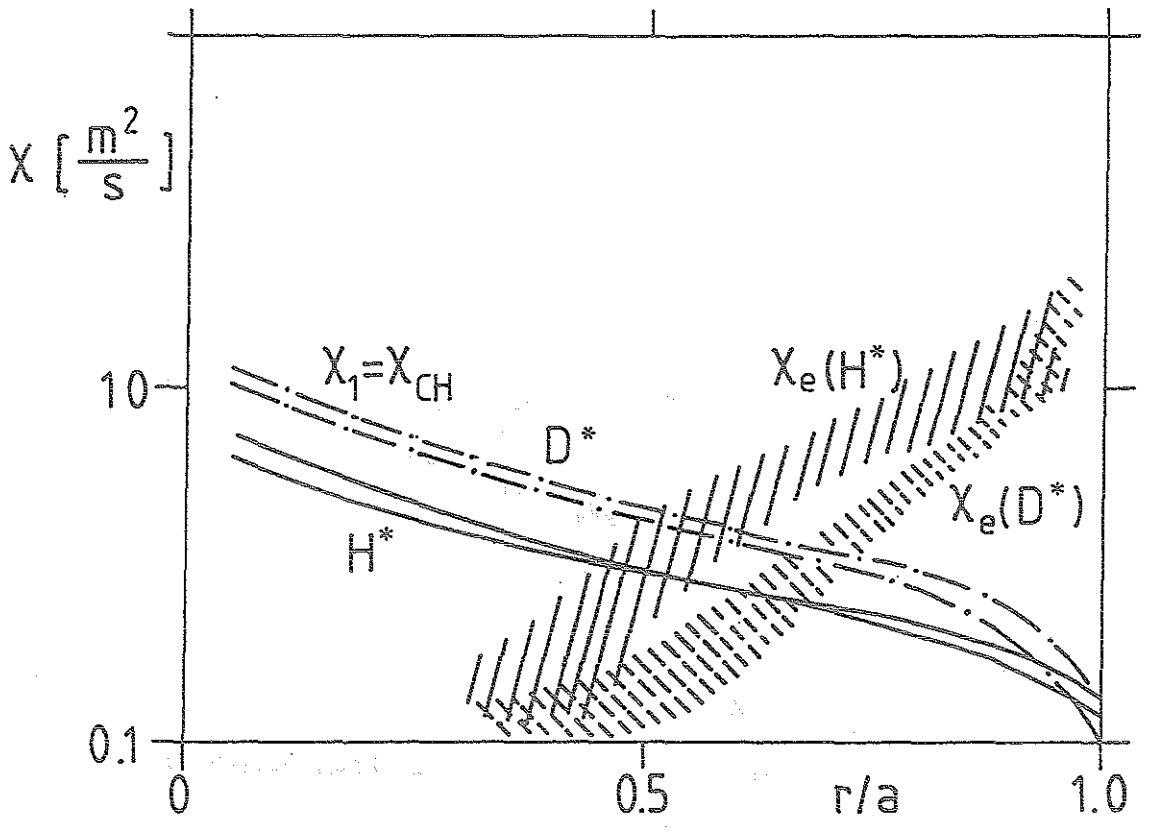

Fig. III.4 Transport coefficients derived by the TRANSP-code for ASDEX /III.C.1/.

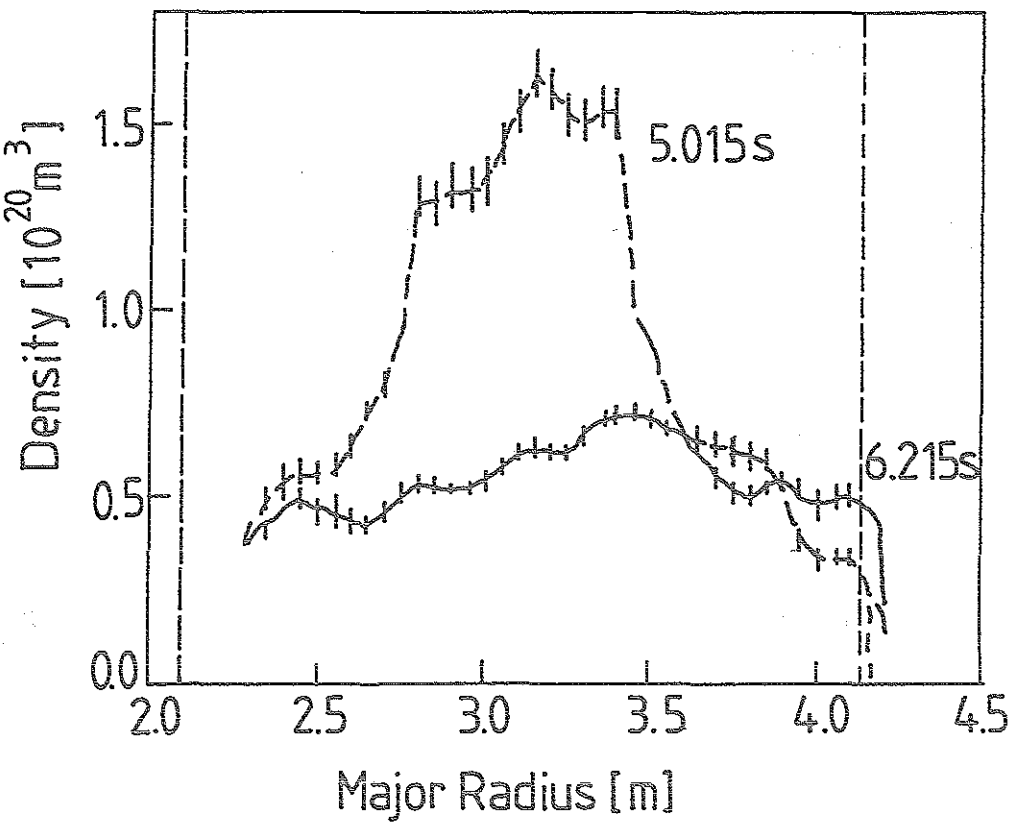

Fig. III.5 Density profile for a PEP-H-mode (top curve) and an H-mode (lower curve) discharge on JET /III.D.2/.

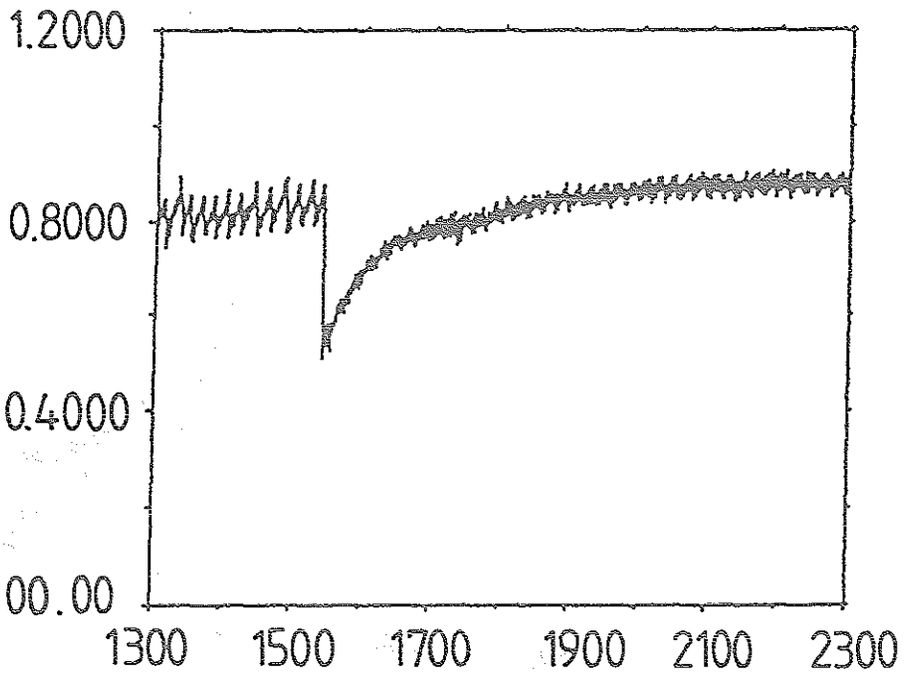

Fig. III.6 Sawtooth activity on TEXTOR before and after pellet injection.

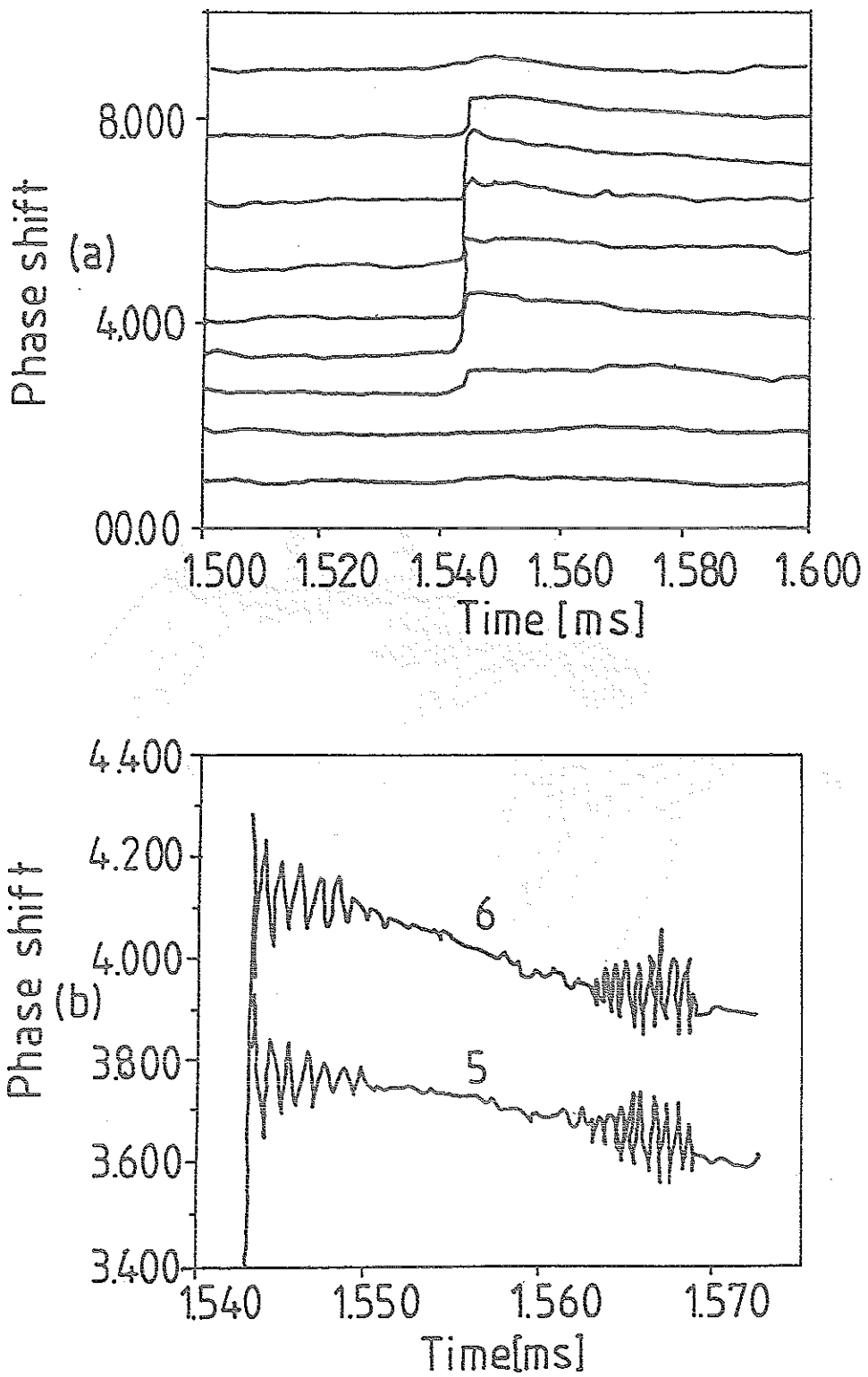

Fig. III.7 a) Fast oscillation of density perturbation after pellet injection. b) Time expansion of a) /III.1.2/.

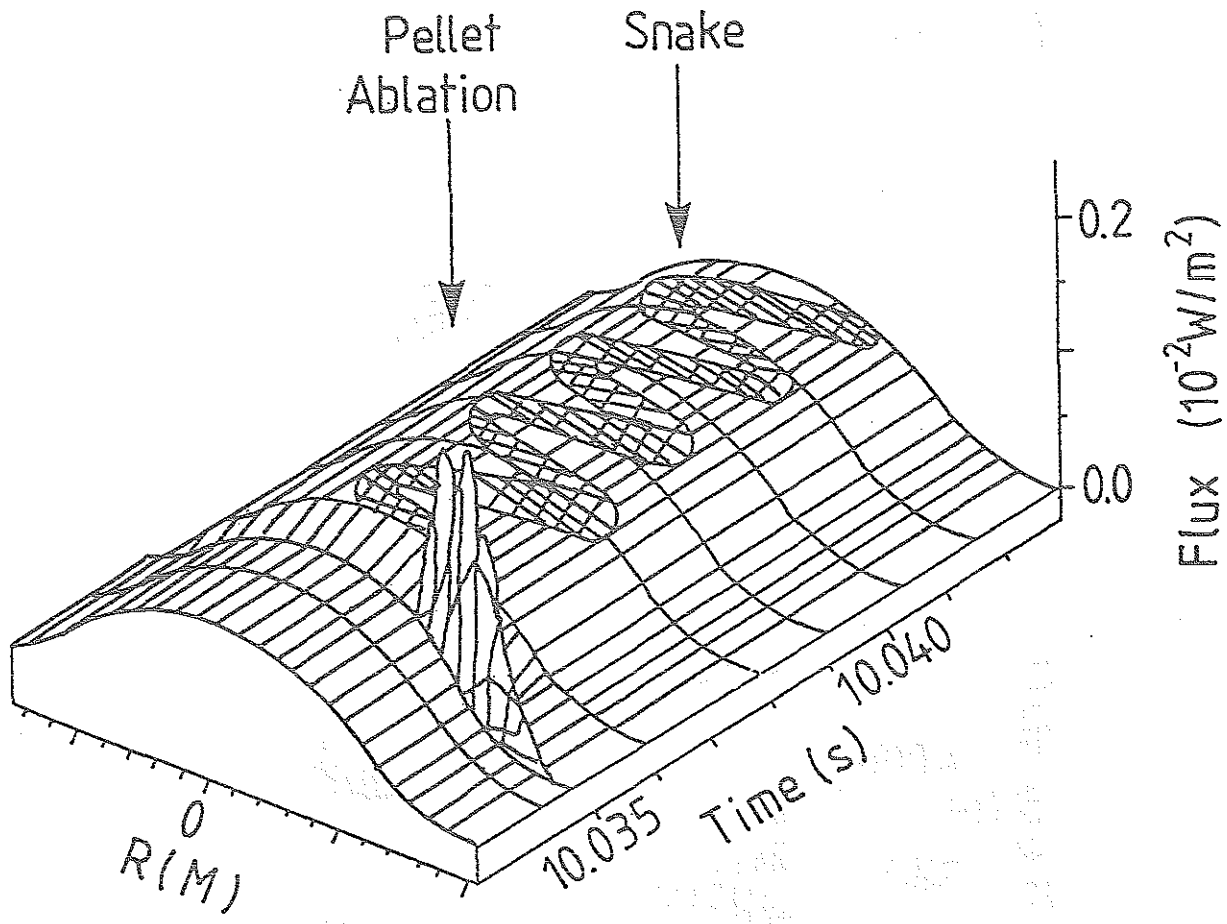

Fig. III.8 Pellet ablation and snake oscillation on JET /III.I.5/.

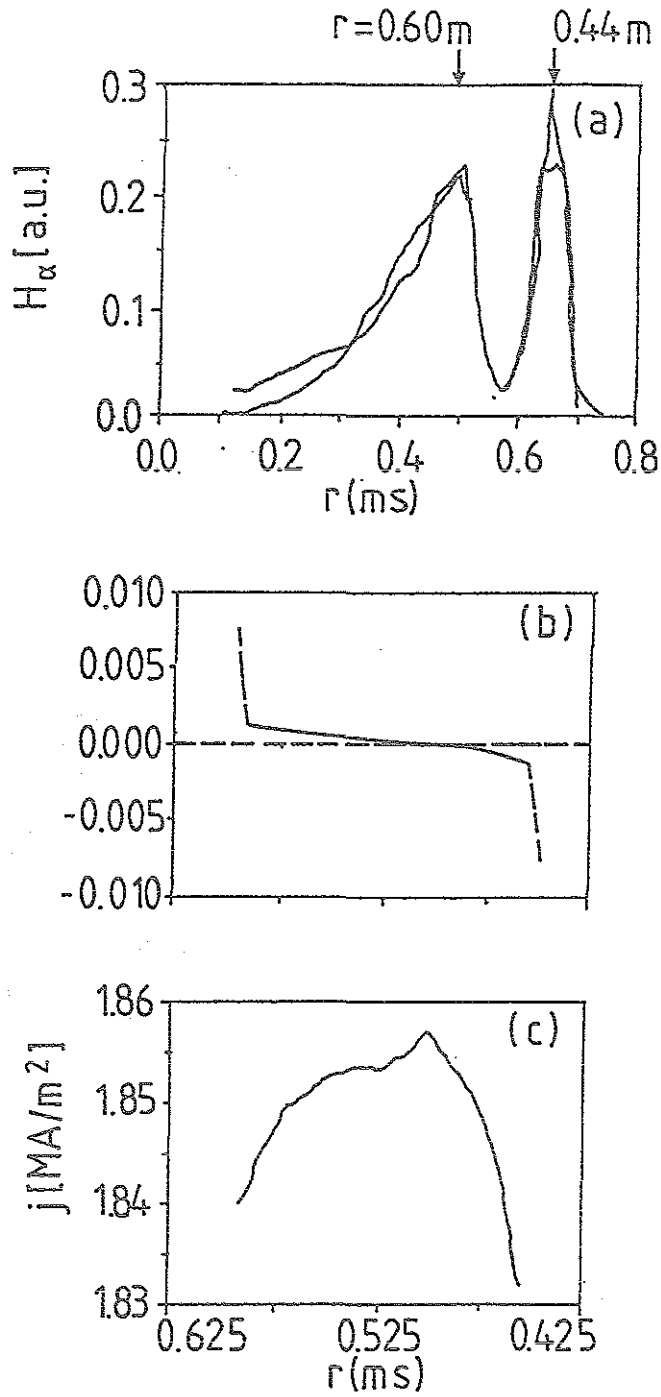

Fig. III.9 a) Comparison between the ablation H_α-signal and the model, b) radial q-variation and c) current distribution /III.J.4/.

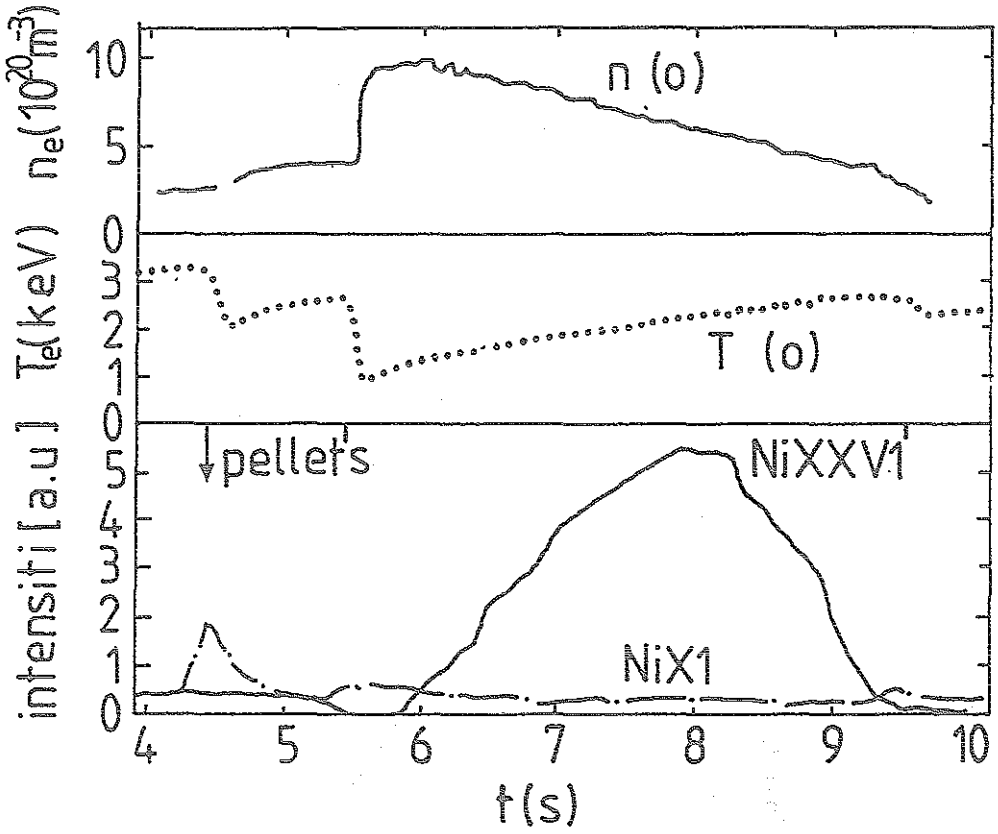

Fig. III.10 Nickel accumulation in pellet discharge. Signals: Density, temperature, and Nickel brilliance (JET, /III.K.1/).

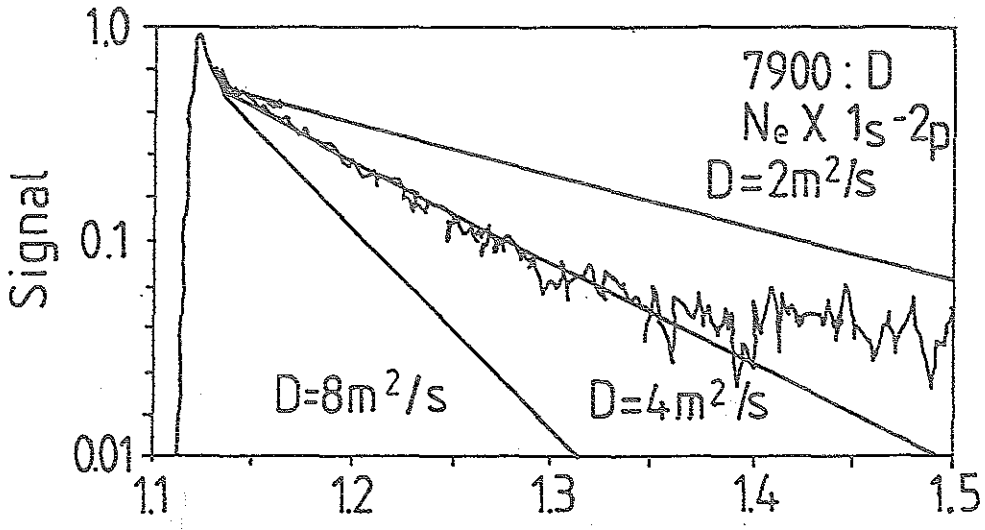

Fig. III.11 Decay of NeX signal after injection of Ne-doped pellet and fitting of transport coefficients (ASDEX, /III.K.4/).

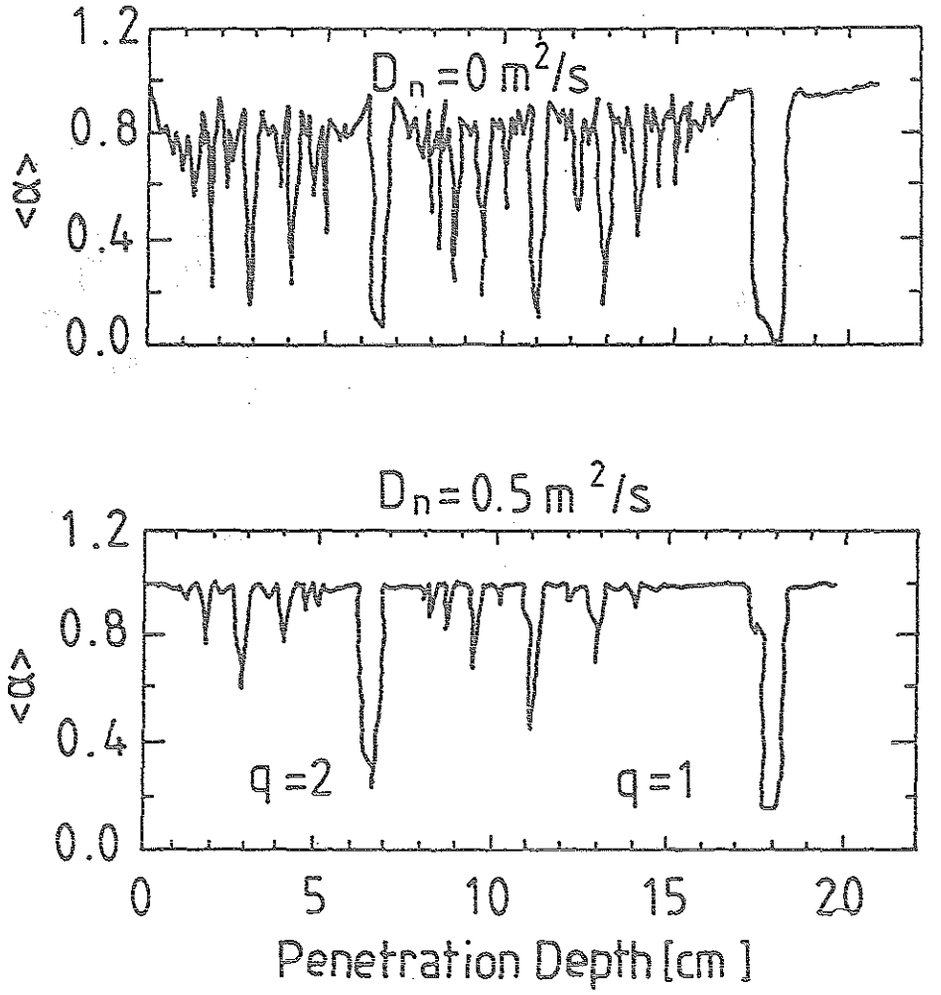

Fig. III.12 Striations of impurity pellet ablation light observed on TEXT. The striations can be attributed to rational q-surfaces /III.K.5/.

FORSCHUNGSZENTRUM JÜLICH GmbH

KFA

Jül-2980
October 1994
ISSN 0944-2952